PTEN differentially regulates endocytosis, migration, and proliferation in the enteric protozoan parasite *Entamoeba histolytica*

Samia Kadri[1, ¶], Kumiko Nakada-Tsukui[2, ¶], Natsuki Watanabe[1], Ghulam Jeelani[1], and Tomoyoshi Nozaki[1, *]

[1]Department of Biomedical Chemistry, Graduate School of Medicine, The University of Tokyo, Tokyo, Japan; [2]Department of Parasitology, National Institute of Infectious Diseases, Tokyo, Japan.

[¶]These authors equally contributed to the work.

*Correspondence: T. Nozaki, nozaki@m.u-tokyo.ac.jp

Author contributions: Conceptualization: KNT and TN; Data curation: SK and KNT; Formal Analysis: SK, KNT, GJ, and NW; Funding Acquisition: KNT, NW, and TN; Investigation: SK, KNT, and NW; Methodology: SK, KNT, NW, and TN; Project Administration: KNT, GJ, and TN; Resources: SK, KNT, NW, GJ, and TN; Supervision: TN; Validation: SK, KNT, and NW; Writing-Original Draft Preparation: SK and TN; Writing-Review and Editing: TN.

Abstract

PTEN is a lipid phosphatase that is highly conserved and involved in a broad range of biological processes including cytoskeletal reorganization, endocytosis, signal transduction, and cell migration in all eukaryotes. Although regulation of phosphatidylinositol (3,4,5)-trisphosphate [PtdIns(3,4,5)P_3] signaling via PTEN has been well established in model organisms and mammals, it remains elusive in the parasitic protist *E. histolytica*, which heavily relies on PtdIns phosphate(s)-dependent membrane traffic, migration, and phago- and trogocytosis for its pathogenesis. In this study, we characterized the major PTEN from *E. histolytica*, EhPTEN1, which shows the highest expression at the transcript level in the trophozoite stage among 6 possible PTENs, to understand the significance of PtdIns(3,4,5)P_3 signaling in this parasite. Live imaging of GFP-EhPTEN1 expressing amebic trophozoites showed localization mainly in the cytosol with a higher concentration at pseudopods and the extending edge of the phago- and trogocytic cups. Furthermore, quantitative analysis of phago- and trogocytosis using a confocal image cytometer showed that overexpression of EhPTEN1 caused reduction in trogo- and phagocytosis while transcriptional gene silencing of *EhPTEN1* gene caused opposite phenotypes. These data suggest that EhPTEN1 has an inhibitory role in these biological processes. Conversely, EhPTEN1 acts as a positive regulator for fluid-phase and receptor-mediated endocytosis in *E. histolytica* trophozoites. Moreover, we showed that EhPTEN1 was required for optimal growth and migration of this parasite. Finally, the phosphatase activity of EhPTEN1 towards PtdIns(3,4,5)P_3 was demonstrated, suggesting that the biological roles of EhPTEN1 are likely linked to its catalytic function. Taken together, these results indicate that EhPTEN1 differentially regulates multiple cellular activities essential for proliferation and pathogenesis of the organism, via PtdIns(3,4,5)P_3 signaling. Elucidation of biological roles of PTEN and PtdIns(3,4,5)P_3 signaling at the molecular

levels promotes our understanding of the pathogenesis of this parasite and potentially leads to the design of novel therapeutics against amebiasis.

Author summary

Entamoeba histolytica is an intestinal protozoan parasite that causes amoebic dysentery and liver abscesses in humans. It has been well understood how the amoeba's ability to ingests and destroy human cells and invade tissues contributes to disease symptoms such as bloody diarrhea. The underlying mechanisms for such activities, called pathogenicity, include trafficking (transport) and secretion of cytolytic proteins, migration (ameboid movement), and ingestion and destruction of human cells, heavily rely on the signal transduction system via metabolism (synthesis and decomposition) of phosphoinositides (phosphatidylinositols containing 0-5 phosphates), and downstream regulation of cytoskeleton (dynamic network of interlinking protein filaments, such as actin, in the cytoplasm). In this study, we characterized one enzyme called EhPTEN1, which degrades and inactivate PtdIns(3,4,5)P_3. We have shown that EhPTEN1 is involved in migration, internalization of soluble and solid materials (endocytosis, trogo-, and phagocytosis). EhPTEN1 apparently regulates cell migration, endocytosis, trogo-, phagocytosis, and proliferation in a complex fashion. Our findings help in the elucidation of the physiological significance of PTEN and cellular events regulated via phosphoinositides in this enteric parasite and other pathogenic parasites, and potentially lead to the development of new control measures against parasitic diseases.

Introduction

Phosphatidylinositol phosphates (PIPs) are membrane phospholipids that play pivotal roles in a variety of biological processes such as cytoskeletal reorganization, vesicular trafficking, endocytosis, signal transduction, ion channel activation, and cell migration [1,2]. There are seven different species of PIPs in mammalian cells including three phosphatidylinositol monophosphate, three phosphatidylinositol biphosphate, and one phosphatidylinositol triphosphate [2]. PIPs kinases and phosphatases regulate the cellular function of PIPs through reversible phosphorylation and de-phosphorylation [3]. PTEN (phosphatase and tensin homologue) is a lipid phosphatase that dephosphorylates phosphatidylinositol (3,4,5)-trisphosphate [PtdIns(3,4,5)P_3] to phosphatidylinositol (4,5)-bisphosphate [PtdIns(4,5)P_2], thus depleting cellular signaling processes downstream of PtdIns(3,4,5)P_3 [4]. PtdIns(3,4,5)P_3 acts as a secondary messenger which activates the proto-oncogenic PI3K–AKT signaling pathway [5]. PTEN plays a crucial role in cell proliferation through its cytoplasmic phosphatase activity against the PI3K–AKT cascade [6]. Also, PTEN regulates cell polarity and migration via the establishment of a PtdIns(3,4,5)P_3-PtdIns(4,5)P_2 gradient [7,8]. Many human cancers are associated to PTEN mutations, including endometrial tumors, glioblastoma, prostate carcinoma, melanoma, and hereditary cancer predisposition syndromes, such as Cowden disease [9,10]. Furthermore, PTEN can modulate immune responses by regulating Fcγ receptor-mediated phagocytosis [11,12].

Human amebiasis is caused by the infection of the enteric protozoan parasite *Entamoeba histolytica*. World Health Organization estimates 50 million people throughout the world suffers from amebic infections, resulting in around 100,000 deaths annually [13]. Infection by *E. histolytica* usually occurs via ingestion of fecally contaminated food or water with the infective cyst of this parasite [14]. Destruction of intestinal epithelial tissue by amoebic trophozoites causes colitis and amoebic dysentery while in some patients trophozoites can infect extraintestinal organs

where they form abscesses [15]. It is known that the virulence mechanisms of *E. histolytica* are sustained by actin-associated processes such as migration, adhesion, and trogo-/phagocytosis as well as vesicular traffic involved in the secretion of proteases [16-19]. A sufficient set of PI-kinases and phosphatases to generate 7 species of phosphoinositides appear to be conserved in *E. histolytica* [20]. AGC kinases have recently been identified as PtdIns(3,4,5)P_3-binding proteins and shown to be involved in trogocytosis and phagocytosis in *E. histolytica* [21]. Physiological significance of PtdIns(3)P- and PtdIns(4)P-binding proteins including FYVE domain-containing proteins was shown [22]. In addition, the distinct roles of PtdIns(3)P-binding sorting nexins (SNXs) in trogocytosis have been demonstrated in *E. histolytica* [23]. Among them, PtdIns(3,4,5)P_3-mediated signaling is assumed to have a pivotal role in *E. histolytica* virulence. Although physiological roles of PTEN have been well established in higher eukaryotes, the role of PTEN in *E. histolytica* in pathogenesis remains elusive.

In the present study, we characterized the biological roles of EhPTEN1, which shows the highest expression at the transcript level in the trophozoite stage among six putative PTENs encoded by the genome. We have shown that EhPTEN1 is enzymatically active against PtdIns(3,4,5)P_3 and is required for optimal growth of *E. histolytica* cells. We have also found that EhPTEN1 is involved in the regulation of different modes of endocytosis, namely fluid-phase endocytosis, receptor-mediated endocytosis, phago-, trogocytosis, and cell migration.

Results

Identification and features of *PTEN* genes in *E. histolytica*

A genome-wide survey of PTEN in the genome of *E. histolytica* HM-1:IMSS reference strain (AmoebaDB, http://amoebadb.org) by BLASTP analysis using human PTEN (P60484) as a query,

revealed that *E. histolytica* possesses 6 possible PTEN or PTEN-like proteins that contain PTEN phosphatase domain, and show different domain configurations (Fig 1A) [20]. We tentatively designated them firstly in an ascending order of the number of recognizable domains and secondly in a descending order of the overall length (EhPTEN1, EHI_197010; EhPTEN2, EHI_098450; EhPTEN3, EHI_131070; EhPTEN4, EHI_054460; EhPTEN5, EHI_041900; EhPTEN6, EHI_010360). Our previous transcriptome data [24-26] verified that one protein (EhPTEN1, EHI_197010) is highly expressed in the trophozoite stage in both *E. histolytica* HM-1: IMSS cl6 and G3 strains, while the 5 other PTENs are expressed at relatively low levels (Fig 1B). EhPTEN1 shows 39% mutual identity to human PTEN at the amino acid level (S1 Table). Multiple sequence alignment by ClustalW program (http://clustalw.ddbj.nig.ac.jp) shows that the key catalytic residues in the phosphatase domain (H-C-K/R-A-G-K-G-R) needed for lipid and protein phosphatase activity [4,27] are well conserved in EhPTEN1 (Fig 1C). In addition, the PtdIns(4,5)P_2-binding motif (K/R-x4-K/R-x-K/R-K/R-R, PDM domain), which is predicted to regulate the recruitment of protein to the plasma membrane, located at the amino terminus, is also conserved in EhPTEN1 [6,28]. The cytosolic localization signal (D-G-F-x-L-D-L, CLS), where mutation of phenylalanine was shown to induce nuclear localization [29], as well as threonine and isoleucine responsible for TI loop formation in an extension of the active site pocket are also conserved (Fig 1C) [27]. EhPTEN1 also possesses C2 domain which has an affinity for membrane phospholipids and helps PTEN to be recruited to the cell membrane [27]. InterPro domain search annotates the region of a.a. 550-680 of EhPTEN1 as a domain of unknown function (DUF457). The two PEST sequences, rich in proline, glutamic acid, serine, and threonine, at the C terminus of human PTEN, are not conserved in EhPTEN1. Although PEST sequences are known to enhance proteolytic sensitivity, the regulation of EhPTEN1 functions may differ from the human PTEN

[30]. EhPTEN1 also lacks PDZ-binding motif (T/S-x-V) located at the C-terminal end in human PTEN and facilitates the protein-protein interactions [6,31]. The ~400 a.a. carboxyl-terminal extension which is absent in human ortholog and rich in charged amino acids could be involved in regulating its protein-protein interactions.

Cellular localization and dynamics of EhPTEN1 in the motile *E. histolytica* trophozoite

To examine the cellular localization of EhPTEN1 in trophozoites, we established a transformant line expressing EhPTEN1 with the GFP-tag at the amino terminus (GFP-EhPTEN1). The expression of GFP-EhPTEN1 or GFP (control) in transformant trophozoites was verified by immunoblot analysis using anti-GFP antibody. A single band corresponding to non-truncated GFP fusion protein with an expected molecular mass of GFP-EhPTEN1 (90 kDa plus 26 kDa for the GFP tag) was observed in the GFP-EhPTEN1-expressing transformant (Fig 2A). Live imaging analysis revealed that GFP-EhPTEN1 was localized throughout the cytosol (Fig 2B and S1 Movie). The line intensity plots across the GFP-PTEN1 overexpressing trophozoites further demonstrated the enrichment of GFP-PTEN1 along the extended pseudopod of the motile trophozoite (Fig 2B) (Two additional images are also show in S1A and S1B Fig). The normalized average fluorescence intensities at the leading regions of pseudopods were nearly 1.5-fold higher in GFP-EhPTEN1 overexpressing trophozoites compared to mock transformants (Fig 2C). Furthermore, the intensity line plot of GFP-expressing control strain showed no accumulation of GFP signal on pseudopods (S2 Fig and S2 Movie). These findings confirm the enrichment of GFP-EhPTEN1 in the pseudopod-like protrusive structures. Similarly, immunofluorescence imaging of HA-EhPTEN1 overexpressing trophozoites using anti-HA antibody revealed that HA-EhPTEN1 was localized in the cytoplasm in steady-state, and enriched in pseudopods (S3B and S3C Fig). The migration (motility) of the GFP-EhPTEN1 overexpressing trophozoites using the montage of time-lapse

159 imaging was 0.54±0.09 μm/sec (mean±S.D.), which was significantly greater than that of control
160 GFP expressing transformants (0.27±0.08 μm/sec) (Fig 2D). We also investigated the effect of
161 repression of *EhPTEN1* gene expression and found that *EhPTEN1* gene silencing reduced
162 migration (see below).

163 **Localization of EhPTEN1 during trogocytosis and phagocytosis**

164 The fact that EhPTEN1 was previously identified as a PtdIns(3)P-binding effector and suggested
165 to be involved in the phagosome biogenesis [23], prompted further characterization of the role of
166 EhPTEN1 in host cell internalization. To examine the role of EhPTEN1 in ingestion of mammalian
167 cells, we first examined trogocytosis (i.e., nibbling or chewing of a part of a live cell) of Chinese
168 hamster ovary (CHO) cells by GFP-EhPTEN1 and GFP expressing transformant lines. We co-
169 cultured trophozoites of the two transformant lines with live CHO cells that had been stained with
170 CellTracker Orange. Time-lapse imaging of trogocytosis of CHO cells by the amoebae (Fig 3A
171 and S3 Movie) revealed that GFP-EhPTEN1 was accumulated in the region that covers, but not
172 always in close proximity to, the tunnel-like structure, which is the extended neck (or tube)-like
173 structure connecting the enclosed (or being enclosed) trogosome and the remaining portion of the
174 target cell that is partially ingested (Fig 3A-3D). Upon completion of closure of the trogosome,
175 GFP-EhPTEN1 appeared to be dissociated from the region around the trogosome and the tunnel-
176 like structure (Fig 3A-3E). The quantification of the fluorescence intensity in a cross section of the
177 cell confirmed the dynamism of GFP-EhPETN1 during trogocytosis (Figs 3B-3E). In contrast, at
178 the very early phase of trogocytosis, GFP-EhPTEN1 was not concentrated on the newly formed
179 trogocytic cup.

180 The dynamics of GFP-EhPTEN1 in a course of phagocytosis (i.e., internalization with a
181 single bite, not multiple bites) of dead CHO cells was also examined. The live imaging of GFP-

EhPTEN1 expressing trophozoites co-cultured with pre-killed CHO cells (Fig 4 and S4 Movie) showed an enrichment of GFP-EhPTEN1 at the tip of the leading edge of the phagocytic cup during the internalization of dead host cells until phagosome closure (Fig 4A and 4B). Soon after closure of the phagosome, GFP-EhPTEN1 was concentrated on the closing side of the phagosome (Fig 4A-4C), and rapidly disappeared soon after (Fig 4D). The fluorescence intensity line plot of a cross section (as indicated by arrows) of the cell also reinforced the observation (Figs 4A-4D). As control, GFP-expressing mock strain showed no observable concentration of GFP signal in a course of CHO ingestion (S5 Movie and S4 Fig).

Effect of overexpression of EhPTEN1 on trogocytosis and phagocytosis

The dynamism of GFP-EhPTEN1, as revealed by live imaging, suggests that EhPTEN1 plays a role in the early to middle stages of trogo- and phagocytosis. We examined the effect of GFP-EhPTEN1 overexpression on the efficiency (i.e., speed and volume of internalization of prey) of trogocytosis and phagocytosis. GFP-EhPTEN1 expressing and mock transformant strains were incubated with either live or pre-killed CHO cells that had been stained with CellTracker Orange to allow trogocytosis or phagocytosis, respectively. Internalization of CHO cells by the amoebae was measured by CQ1 confocal quantitative image cytometer (Figs 5 and 6). Three parameters were measured and compared between GFP-EhPTEN1 expressing and mock transformant strains: the number of CHO-containing trogosomes or phagosomes per ameba (Figs 5A and 6A), the volume of all CHO-containing trogosomes or phagosomes per ameba (Figs 5B and 6B), and the percentage of the amebae that ingested CHOs (Figs 5C and 6C). GFP-EhPTEN1 overexpression caused statistically significant reduction in all three parameters in both trogocytosis and phagocytosis.

Gene silencing of *EhPTEN1* enhances trogocytosis and phagocytosis in *E. histolytica*

Conversely, we attempted to verify if repression of *EhPTEN1* gene expression by antisense small RNA-mediated transcriptional gene silencing [32] causes reverse phenotypes: enhancement of trogocytosis and phagocytosis. The silencing of the *EhPTEN1* gene expression was confirmed by RT-PCR and the level of silencing was estimated to be approximately 77.0±9.2% compared to the mock control (G3 transfected with the empty psAP2-Gunma vector) (Fig 7A and 7B). Non-specific off-target gene silencing of other *EhPTEN* genes (*EhPTEN2-6*) was ruled out, except for *EhPTEN2*, which showed a slight reduction in *EhPTN1* gene silenced strain, validating gene-specific silencing (S5 Fig). The *RNA pol II* transcript level was also unaffected. *EhPTEN1* gene silenced and mock transformants were cultivated with live or dead CHO cells and images were captured every 10 min for 1 hr. As expected, *EhPTEN1* gene silenced strain showed an enhancement of trogocytosis and phagocytosis (Fig 8). All three parameters to evaluate trogocytosis and phagocytosis, as above, i.e., the number of CHO-containing trogosomes or phagosomes per ameba (Figs 8A and 8B), the volume of all CHO-containing trogosomes or phagosomes per ameba (Figs 8C and 8D), and the percentage of the amebae that ingested CHOs (Figs 8E and 8F) was significantly increased in EhPTEN1gene silenced strain compared to the mock control stain. For instance, the volume of trogosomes and phagosomes increased by around 1.4 fold for trogocytosis and 2 fold for phagocytosis, respectively, in EhPTEN1gene silenced strain at later time points of coincubation (at 40-60 mins). Together with the results of EhPTEN1 overexpression, shown above, these data indicate that EhPTEN1 serves as a negative regulator of trogocytosis and phagocytosis.

EhPTEN1 is a positive regulator for the fluid-phase and receptor-mediated endocytosis in *E. histolytica*

To investigate the role of EhPTEN1 in pinocytosis of the fluid-phase marker and receptor-mediated endocytosis, we examined the internalization of RITC dextran and transferrin.

Pinocytosis was analyzed by measuring, on a fluorometer, the fluorescence intensity of fluid-phase marker, RITC dextran, which was internalized after incubation of amoebic transformants with RITC dextran at 35°C for up to 1 hr. Overexpression of GFP-EhPTEN1 cause approximately 30% increase in pinocytosis in comparison to mock control (53±5.3 or 28±13% at time 30 or 60 min, respectively; $p<0.05$, Fig 9A). Conversely, *EhPTEN1* gene silenced strain showed an approximately 30% decrease in pinocytosis at 30-60 min, as compared to mock control cells (30±8.2 or 25±5.1% decrease at time 30 or 60 min, respectively, $p<0.05$, Fig 9B).

We next examined internalization of transferrin conjugated with AlexaFluor 568 by CQ1 image cytometer. Transferrin is presumed to be internalized via receptor-mediated endocytosis. The volume of endosomes that contained transferin-AlexaFluor 568 increased by 30-50% in GFP-EhPTEN1 overexpressing trophozoites compared to mock control at all time points up to 1 hr ($p<0.05$, Fig 10A). Conversely, transferrin endocytosis decreased by 30-40% in *EhPTEN1* gene silenced strain compared to the mock strain at 40-60 mins ($p<0.05$, Fig 10B). These data indicate that EhPTEN1 positively regulates pinocytosis of the fluid-phase maker and receptor-mediated endocytosis in *E. histolytica*.

EhPTEN1 is essential for optimum growth and migration of *E. histolytica*

The biological role of EhPTEN1 in trogo-, phagocytosis, and endocytosis was clearly demonstrated as above. To investigate other physiological roles of EhPTEN1 in *E. histolytica*, the growth kinetic was monitored in *EhPTEN1* gene silenced and control strains. *EhPTEN1* gene silencing caused significant growth defect: the population doubling time of *EhPTEN1* gene silenced and control strains was 28.1±0.41 and 19.1±0.52 hr, respectively ($P<0.05$; Fig 7C). We next examined the migration of the trophozoites of *EhPTEN1* gene silenced and control strains

using time lapse imaging by CQ1. The velocity of motility was >60% reduced in *EhPTEN1* gene silenced strain (0.16±0.07 µm /min) compared to the mock control (0.44±0.08 µm /min) (Fig 7D).

Demonstration of phosphatase activity and substrate specificity of EhPTEN1

To see if EhPTEN1 possesses lipid phosphatase activity, bacterial recombinant EhPTEN1 with the histidine tag at the amino terminus was produced using the pCOLD I *E. coli* expression system. SDS-PAGE analysis followed by Coomassie Brilliant Blue staining showed that the purified recombinant EhPTEN1 was apparently homogenous with the predicted molecular mass of 96 kDa including the histidine tag (S6A Fig). Immunoblot analysis of the purified recombinant protein using His-Tag antibody confirmed the absence of truncation (S6B Fig). We first examined the enzymatic activities of recombinant EhPTEN1 using a variety of phosphoinositides (PIs) as substrates. EhPTEN1 revealed reasonable activity in a broad pH range with maximum activity obtained at pH 6.0 when the reaction was performed with 50 µM PtdIns(3,4,5)P_3 at 37°C for 40 min (S6C Fig). We then determined the substrate specificity of EhPTEN1, using a panel of di-C8 PIs. EhPTEN1 showed highest activity with PtdIns(3,4,5)P_3 with the apparent specific activity of 8.18±0.78 nmol/min/mg (Fig 11). EhPTEN1 also catalyzed dephosphorylation of PtdIns(3,4)P_2 and PtdIns(3,5)P_2 with 6 or 3 fold lower specific activities, respectively, compared to that toward PtdIns(3,4,5)P_3. The activities against PI monophosphates and PtdIns(4,5)P_2 were relatively low. All these characteristics are similar to those of human PTEN [33,34]. A comparison of kinetic parameters of EhPTEN1 reveals a higher affinity towards PtdIns(3,4,5)P_3 (Km=92.5 ± 4.72 µM) as compared to PtdIns(3,4)P_2 (292 ± 18.8 µM) and PtdIns(3,5)P_2 (161 ± 20.1) demonstrating that in vitro is as well the preferred substrate (Table 1, S8 Fig).

Table 1. Kinetic parameters of EhPTEN1.

Substrate	Km (μM)	Vmax (nmoles min^{-1} mg^{-1})	Kcat (min^{-1})
$PI(3,4)P_2$	292 ± 18.8	6.02 ± 1.11	0.11 ± 0.02
$PI(3,5)P_2$	161 ± 20.1	8.40 ± 0.42	0.15 ± 0.01
$PI(3,4,5)P_3$	92.5 ± 4.72	16.9 ± 1.83	0.31 ± 0.03

Assay was performed as described in Materials and methods in the presence of MOPS, EhPTEN1, and PtdInsPs. Reaction was conducted at 37ºC at pH 6.0. Mean ± SEM of duplicates are shown.

Demonstration of phospholipid binding of EhPTEN1

The lipid overlay assay using amebic lysates from GFP-EhPTEN1 expressing and mock transformants showed that EhPTEN1 preferentially bound to PtdIns(3)P, PtdIns(4)P, PtdIns(5)P, and, to a lesser extent, $PtdIns(3,5)P_2$, and $PtdIns(4,5)P_2$ (S7 Fig). Furthermore, recombinant His-tagged EhPTEN1 also revealed a similar binding affinity toward a panel of PIs on the membrane, which is similar to the data given for recombinant human PTEN [35].

Discussion

PTEN regulates fundamental roles in higher eukaryotes including cell survival, metabolic changes, cell polarity, and migration [9]. In this study, we have characterized the pivotal functions of EhPTEN1 in migration, endocytosis, and cellular proliferation in *E. histolytica*. Confocal live imaging demonstrated the involvement of EhPTEN1 in the initial and intermediate stages of trogocytosis and phagocytosis. In trogocytosis of a live mammalian cell, EhPTEN1 was enriched in the region where the trogocytic tunnel was newly formed. Similarly, EhPTEN1 was accumulated on the cell periphery close to the leading edge of the phagocytic cup during the internalization of a dead host cell. The recruitment of EhPTEN1 was transient as it gradually

296 became dissociated from the region after the completion of ingestion. These results are in line with
297 the previous study that showed PTEN was associated with forming IgG conjugated zymosan
298 containing phagosomes but disappeared once particle ingestion was completed [36]. The
299 biochemical analysis showed that GFP-EhPTEN1 overexpression caused a reduction in
300 trogocytosis and phagocytosis. In good agreement with these results, knockdown of EhPTEN1
301 caused remarkable enhancement in phagocytosis of dead CHO cells while trogocytosis toward live
302 CHO cells was slightly increased. These results match those observed in earlier studies where
303 PTEN deficient macrophages displayed enhanced phagocytic ability both in vitro and in vivo,
304 while overexpression of PTEN significantly inhibited phagocytosis in macrophages [12,37-39]. It
305 was previously demonstrated that PTEN down-regulates phagocytosis through dephosphorylation
306 of PtdIns(3,4,5)P_3, which subsequently affects the downstream events such as the activation of
307 Rac through the pleckstrin homology domain-containing guanine-nucleotide exchange factor,
308 Vav1 [12]. The depletion of PTEN in macrophage resulted in elevated PtdIns(3,4,5)P_3 levels,
309 leading to activation of Vav1 and subsequent activation of Rac1 GTPase, the latter of which
310 induces F-actin polymerization, which in turn enhances the engulfment of targeted cells [40].
311 Furthermore, it has been shown that PTEN negatively regulates Fcγ receptor-mediated
312 phagocytosis by repressing the conversion of Rac-bound GDP to GTP downstream [11]. While
313 PIPs-mediated signaling and downstream effector in *E. histolytica* is not yet well understood, it
314 has been recently reported that two AGC kinases from *E. histolytica* have the ability to bind
315 PtdIns(3,4,5)P_3 and are involved in a panel of endocytic events including trogo-, phago-, and
316 pinocytosis [21]. In addition, it has also been shown that PtdIns(4,5)P_2 is localized on the plasma
317 membrane whereas PtdIns(3,4,5)P_3 is localized on the phagocytic cup and the extended
318 pseudopodia in *E. histolytica* trophozoites [41,42]. These observations suggest that the control of

PtdIns(3,4,5)P_3 synthesis and decomposition are important for the regulation of endocytic events in *E. histolytica*. We have clearly demonstrated phosphatase activity and preferred substrate specificity toward PtdIns(3,4,5)P_3 of EhPTEN1. Hence, it is highly conceivable that EhPTEN1 can regulate the local concentrations of PtdIns(4,5)P_2 and PtdIns(3,4,5)P_3 at the target sites during trogo- and phagocytic processes. It seems conceivable that EhPTEN1 negatively regulates trogo- and phagocytosis by reducing the local PtdIns(3,4,5)P_3 concentration, leading to the suppression of actin-dependent cytoskeletal reorganization needed for trogo- and phagocytosis. Indeed, the concentration of EhPTEN1 is swiftly reduced on and close to trogo- and phagocytic cups (not-yet-enclosed) and trogosomes and phagosomes (enclosed) soon after the completion of ingestion.

We have shown that EhPTEN1 is involved in receptor-mediated endocytosis and macropinocytosis of the fluid-phase marker in an opposite fashion as in trogo- and phagocytosis. GFP-EhPTEN1 overexpression enhanced transferrin uptake while *EhPTEN1* gene silencing decreased it. It was shown that at least two concentration-dependent mechanisms for transferrin endocytosis exist in *E. histolytica* [43]: Receptor-mediated endocytosis active at low transferrin concentrations [44] and receptor-independent internalization at high transferrin concentrations [45]. As previously demonstrated, receptor-mediated endocytosis of transferrin in *E. histolytica* is indeed clathrin-mediated [clathrin-mediated endocytosis (CME)] [46], and receptor-mediated endocytosis is in general clathrin-mediated and actin independent [47]. Unlike trogo- and phagocytosis, CME is also distinct in that it depends on PtdIns(4,5)P_2 and does not require PtdIns(3,4,5)P_3 [47,48]. PtdIns(4,5)P_2 binds and recruits several proteins associated with CME formation thus depleting cells of PtdIns(4,5)P_2 prevents transferrin receptor endocytosis [1,47-49]. Taken together, EhPTEN1 possibly facilitates the transferrin internalization through augmentation of PtdIns(4,5)P_2 synthesis. Furthermore, EhPTEN1 showed similar phenotypes toward pinocytosis

of the fluid-phase marker. As stated above, transferrin, when present at high concentrations, is internalized by receptor independent fashion in *E. histolytica* [45]. Thus, it is consistent with our observation that *E. histolytica* internalization of the fluid-phase marker and transferrin by actin-dependent macropinocytosis (S7 and S8 Movies), also as previously shown [50]. We also previously showed that EhAGCK2, which preferentially binds PtdIns(3,4,5)P_3 over PtdIns(4,5)P_2, is involved in pinocytosis of the fluid-phase marker [21], supporting the actin-dependence of macropinocytosis. However, it was shown that the local production of PtdIns(4,5)P_2 in the early stages of macropinocytosis is essential for the formation of ruffles and is partly responsible for the remodeling of the actin cytoskeleton [51]. Although phagocytosis and macropinocytosis both construct a cup in an actin-dependent manner, phagocytosis is a receptor-guided zipper-like model that conforms to particle geometry while macropinocytosis is self-organized with little or no guidance from receptors and can form in the absence of particles [52]. Moreover, a number of previous studies have shown that macropinocytosis and phagocytosis are distinct. For instance, RacC or Rap1 overexpressing cells or profilin-null cells displayed a higher phagocytosis rate but macropinocytosis was significantly reduced [53-55]. It has been reported previously that deletion of PTEN in *Dictyostelium discoideum* caused a reduction in fluid uptake [56]. Nevertheless, the lipid rafts in the plasma membrane of *E. histolytica* is highly enriched with PtdIns(4,5)P_2 [42] and disruption of lipid rafts with cholesterol-binding agents significantly inhibited fluid-phase pinocytosis of *E. histolytica* [57]. Altogether, we assume that EhPTEN1 accelerates transient synthesis of PtdIns(4,5)P_2 on the plasma membrane which in turn facilitates the formation of actin-associated macropinocytic cup. This study has provide the first observation that PTEN is differentially involved in multiple actin-related cytoskeletal activities.

We have shown that repression of gene expression of *EhPTEN1* caused significant growth defect. This phenotype can be possibly explained by reduced ability in nutrient uptake. Furthermore, it was previously demonstrated that the growth defect in *E. histolytica* in low iron medium was rescued by the addition of iron-loaded holo-transferrin, and that holo-transferrin was recognized by an amoebic transferrin receptor and endocytosed via clathrin-coated vesicles [44,58]. These data, taken together, underscore the importance of endocytosis of transferrin for the proliferation of amoebae. Macropinocytosis was previsouly identified as a mechanism by which malignant cells satisfy their unique metabolic needs and hence support cancer progression [59]. In the amoebae, macropinocytosis is the primary and widely used method for feeding [60]. On the other hand, the downstream signaling molecules that correspond to mammalian PTEN and are related to cellular proliferation, such as B cell lymphoma 2 associated agonist of cell death (BAD) and cyclin-dependent kinase inhibitor p27 [5,8], have not yet been identified in *E. histolytica.* Instead, *E. histolytica* possesses two genes encoding TOR-like proteins by biocomputational approach [61]. These data may suggest that regulation of amoebic growth by PTEN is distinct in *E. histolytica*. On the other hand, it was previously shown that loss of PTEN significantly lowered growth in *D. discoideum*, possibly attributable to mislocalization of myosin II during cytokinesis [62,63]. Similarly, myosin II mutants caused reduction in growth and multinucleation in *E. histolytica* [64]. These observations likely support the premise that EhPTEN1 regulates amoebic cell proliferation by regulation of cytokinesis and/or nutrient uptake by macropinocytosis. Furthermore, the requirement of EhPTEN1 for optimum proliferation indicates that *E. histolytica* apparently does not possess compensatory mechanisms for the PIPs dysregulation caused by the loss of EhPTEN1, and thus have posed it as rational drug target.

We have shown that EhPTEN1, in two forms of tagged/fusion proteins, GFP-EhPTEN1 and HA-EhPTEN1, enhances cell migration while repression of *EhPTEN1* gene expression causes inhibition of motility. These observations agree well with the fact that EhPTEN1 was transiently concentrated in newly formed pseudopods. The GFP-EhPTEN1 distribution in *E. histolytica* is similar to the localization of mammalian PTEN, which predominantly shows cytosolic localization and mediates conversion of PtdIns(3,4,5)P_3 to PtdIns(4,5)P_2 through dynamic interaction with the inner face of the plasma membrane [65,66]. It was also shown that in *D. discoideum* the localization of PTEN changed in response to the chemoattractant stimulation via increase in extracellular cAMP. In resting cells, PTEN is uniformly associated with the plasma membrane, but upon chemoattractant stimulation, PTEN transiently dissociates from the membrane and diffuses into the cytosol with accumulation at the rear of the chemotaxis cells [67]. These data suggest that EhPTEN1 is involved in pseudopods formation and motility. In *D. discoideum*, PTEN was also implicated in cell migration as a positive regulator of motility, because an ameba strain lacking PTEN showed a reduction in migration speed and defect in chemotactic efficiency due to disruption of PtdIns(3,4,5)P_3 / PtdIns(4,5)P_2 concentration gradient throughout the cell [68-70]. In contrast, in mammalian cell types including B cells, glioma cells, and fibroblasts, PTEN was shown to inhibit migration [71,8]. The behavioral analysis of *D. discoideum* showed that loss of PTEN caused a reduction in cell motility due to their inability to repress the formation of lateral pseudopodia that misdirect them, compared with wild-type cells, which produce only one large pseudopod at a time [68,69]. In addition, loss of PTEN also resulted in dysregulation of myosin II assembly at the cell cortex, where PTEN prevents the formation of lateral pseudopodia and promotes cell body contraction and posterior retraction in *D. discoideum* [68,72]. PtdIns(4,5)P_2, produced by PTEN, can recruit and activate a wide variety of actin regulatory proteins at the

plasma membrane, thereby controlling motility [1,48]. For example, PtdIns(4,5)P_2 activates N-WASP directly or indirectly through interaction with IQGAP1 which result in promoting actin polymerization by activation of N-WASP–Arp2/3 complex [1,48,73]. Among them, myosin II and Arp2/3 complex are conserved in *E. histolytica,* where myosin II plays a critical role in movement [64,74] and Arp2/3 complex is involved in actin nucleation [75]. Thus, it is conceivable that EhPTEN1 mediates signaling for pseudopod formation and migration through regulation of PtdIns(3,4,5)P_3 metabolism.

In conclusion, we have shown the biological significance of EhPTEN1 in different forms of endocytosis including trogocytosis, phagocytosis, pinocytosis, and clathrin-mediated endocytosis. We have also demonstrated the essentiality of EhPTEN1 in pseudopod formation, motility, and optimal growth of *E. histolytica*. Taken together, these findings emphasize the importance of EhPTEN1 in modulating a plethora of functions in *E. histolytica*. Exploring PTEN functions in *E. histolytica* will hopefully increase our knowledge on the regulation of cellular processes related to actin remodeling through the PIPs signaling pathway. Also, it will inform the rational design of novel therapies against eukaryotic pathogens.

Materials and methods

Identification and comparison of PTEN sequences

Amino acid sequences of PTEN from *E. histolytica* and other organisms were gained from AmoebaDB (http://amoebadb.org/amoeba/) and NCBI (https://www.ncbi.nlm.nih.gov) respectively, and aligned using CLUSTAL W program (http://clustalw.ddbj.nig.ac.jp/) to examine the domain configuration and the key residues for phosphatase activity [76].

Organisms, cultivation, and reagents

Trophozoites of *E. histolytica* clonal strains HM-1:IMSS cl6 and G3 strain were cultured axenically in 6 ml screw-capped Pyrex glass tubes in Diamond's BI-S-33 (BIS) medium at 35.5°C as described previously [77-79]. CHO cells were grown at 37°C in F12 medium (Invitrogen-Gibco, New York, U.S.A.) supplemented with 10% fetal bovine serum on a 10-cm-diameter tissue culture dish (IWAKI, Shizuoka, Japan). *Escherichia coli* BL21 (DE3) strain was purchased from Invitrogen (California, USA). Ni^{2+}-NTA His-bind slurry was obtained from Novagen (Darmstadt, Germany). Rhodamine B isothiocyanate-Dextran (RITC-Dextran) and anti-GFP antibody were purchased from Sigma-Aldrich (Missouri, USA). The anti-HA 16B12 monoclonal mouse antibody was purchased from Biolegend (San Diego, USA). Anti-His antibody was purchased from Cell Signaling Technology (Massachusetts, USA). Lipofectamine, PLUS reagent, and geneticin (G418) were purchased from Invitrogen. CellTracker Green, Orange, and Blue were purchased from Thermo Fisher Scientific (Massachusetts, USA). Restriction enzymes and DNA modifying enzymes were purchased from New England Biolabs (Massachustts, USA) unless otherwise mentioned. Luria Bertani (LB) medium was purchased from BD Difco (New Jersey, USA). Other common reagents were from Wako Pure Chemical (Tokyo, Japan), unless otherwise stated.

Establishment of *E. histolytica* transformants

To construct a plasmid to express EhPTEN1 fused with HA or GFP tag fused at the amino terminus, a DNA fragment corresponding to cDNA encoding EhPTEN1 was amplified by polymerase chain reaction (PCR) from *E. histolytica* cDNA using a pair of primers listed in S2 Table. The PCR-amplified fragments were digested with XmaI and XhoI and cloned into pEhEx-HA and pEhEx-GFP vectors [21,22] that had been predigested with XmaI and XhoI, to produce pEhExHA-EhPTEN1 and pEhExGFP-EhPTEN1. For antisense small RNA-mediated transcriptional silencing of *EhPTEN1* gene, a 420 bp fragment of the protein coding region of *EhPTEN1* gene,

corresponding to the amino terminus of the protein, was amplified by PCR from cDNA with sense and antisense oligonucleotides containing StuI and SacI restriction sites (S2 Table). The amplified product was digested with StuI and SacI and ligated into the compatible sites of the double digested psAP2-Gunma plasmid [80] to synthesize a gene silencing plasmid designated as psAP2-EhPTEN1. Two plasmids, pEhExHA-EhPTEN1 and pEhExGFP-EhPTEN1, were introduced into the trophozoites of *E. histolytica* HM-1:IMSS cl6 strain, whereas psAP2-EhPTEN1 was introduced into G3 strain by lipofection as described previously [81]. Transformants were initially selected in the presence of 1 μg/ml G418 until the drug concentration was gradually increased to 10 μg/ml for the *EhPTEN1* gene silenced stain and 20 μg/ml for the GFP- and HA-EhPTEN1 overexpressing stains. Finally, all transformants were maintained at 10 or 20 μg/ml G418 in BIS medium.

Reverse transcriptase PCR

Reverse transcriptase PCR was performed to check mRNA levels of EhPTEN1 in EhPTEN1 gene silenced and control strains. Total RNA was extracted from trophozoites of EhPTEN1 gene silenced and control strains that were cultivated in the logarithmic phase using TRIZOL reagent (Life Technologies, California, USA). Approximately one μg of DNase treated total RNA was used for cDNA synthesis using Superscript III First -Strand Synthesis System (Thermo Fisher Scientific, Massachusetts, USA) with reverse transcriptase and oligo (dT) primer according to the manufacture's protocol. Ex Taq PCR system was used to amplify DNA from the cDNA template using the primer pairs listed in S2 Table. The PCR conditions were as follow: initial denaturation at 98°C for 10 sec; then 25 cycles at 98°C for 10 sec, 55°C for 30 sec, and 72°C for 20 sec; and a final extension at 72°C for 7 min. The PCR products obtained were resolved by agarose gel electrophoresis.

Immunoblot analysis

Trophozoites of amoeba transformants expressing HA-EhPTEN1 or GFP-EhPTEN1 grown in the exponential growth phase were harvested and washed three times with phosphate buffer saline (PBS). After resuspension in lysis buffer (50 mM Tris-HCl, pH 7.5, 150 mM NaCl, 0.1% Triton-X 100, 0.5 mg/ml E-64, and protease inhibitor), the trophozoites were kept on ice for 30 min, followed by centrifugation at 500 × *g* for 5 min. Approximately 20 µg of the total cell lysates were separated on 10% SDS-PAGE and subsequently electrotransferred onto nitrocellulose membranes. The membranes were incubated in 5% non-fat dried milk in Tris-Buffered Saline and Tween-20 (TBST; 50 mM Tris-HCl, pH 8.0, 150 mM NaCl, and 0.05% Tween-20) for 1 hr at room temperature to block non-specific protein. The blots were reacted with one of the following primary antibodies diluted as indicated: anti-HA 16B12 monoclonal mouse antibody at a dilution of 1:1,000, anti-GFP mouse monoclonal antibody (1:100), and anti-CS1 rabbit polyclonal antisera [82] (1:1,000) at 4°C overnight. The membranes were washed with TBST and further reacted with horseradish peroxidase-conjugated (HRP) anti-mouse or anti-rabbit IgG antisera (1:10,000) at room temperature for 1 hr. After washings with TBST, the specific proteins were visualized with a chemiluminescence HRP Substrate system (Millipore, Massachusetts, USA) using LAS 4000 (Fujifilm Life Science, Cambridge, USA) according to the manufacture's protocol.

Live cell imaging

Approximately 5×10^5 trophozoites of the transformant strain expressing GFP-EhPTEN1 were cultured on a 35 mm (in diameter) collagen-coated glass-bottom dish (MatTek Corporation, Massachusetts, USA) in 3 ml of BIS medium under anaerobic conditions. CHO cells were stained with BIS medium containing 10 µM CellTracker Orange for 40 min followed by washing three times with PBS. Approximately 2×10^4 prestained CHO cells 200 µl BIS were gently overlayed to

trophozoites grown on the glass-bottom dish as prepared above. The central part of the dish was then carefully covered with a 1 cm square coverslip and the edge of the coverslip on the slide glass was sealed with nail polish. Live imaging was performed, images were captured on Zeiss LSM780 confocal microscope, and analyzed by ZEN software (Carl-Zeiss, Oberkochen, Germany).

Indirect immunofluorescence assay (IFA)

Approximately 5×10^3 trophozoites in 50 µl BIS were transferred to an 8 mm round well on a slide glass (Matsunami Glass Ind, Osaka, Japan). After 30 min incubation in an anaerobic chamber at 35.5°C, 5×10^4 CHO cells that had been pre-stained with 10 µM CellTracker Blue in 50 µl BIS were added to the well and the mixture was incubated for 15 min. After removing the medium, cells were fixed with PBS containing 3.7 % paraformaldehyde at room temperature for 10 min, and subsequently permeabilized with PBS containing 0.2% Triton 100-X and 1 % bovine serum albumin (BSA) for 10 min each at room temperature. The cells were then reacted with anti-HA mouse monoclonal antibody (1:1000) for 1 hr at room temperature. Then the sample was reacted with Alexa Flouor-488 conjugated anti-mouse IgG (1:1000) antibody (Thermo Fisher, Massachusetts, USA). The images were then captured using LSM 780 confocal microscope and analyzed by ZEN software (Carl-Zeiss, Oberkochen, Germany).

Trogocytosis and phagocytosis assay using CQ1

Trophozoites of *E. histolytica* were incubated in BIS containing 10 µM CellTracker Blue (Thermo Fisher) at 35.5°C for 1 hr. After staining, ameba trophozoites were washed 3 times with PBS and resuspended in OPTI-MEM medium (Thermo Fisher, Massachusetts, USA) containing 15% adult bovine serum (Sigma Aldrich). Approximately 2×10^4 ameba trophozoites were seeded into a well on a 96-well glass bottom plate (IWAKI, Shizuoka, Japan) and incubated in anaerobic chamber for 40 min. After incubation, about 1×10^5 live or heat killed CHO cells that have been stained with

10 µM CellTracker Orange were added to the well containing amebae. The images were taken on a Confocal Quantitative image cytometer CQ1 (Yokogawa Electric Corporation, Tokyo, Japan) using 20× objective every 10 min for 1 hr. The images were analyzed using CellPathfinder software (Yokogawa Electric Corporation, Tokyo, Japan) according to the manufacture's protocol. The multiple parameters were measured to evaluate the efficiency of trogocytosis and phagocytosis: the average number of internalized CHO cells per amoeba, the combined volume of internalized CHO cells per amoeba, and the percentage of amebic trophozoites that ingested the target cells in the whole population.

Measurement of fluid-phase and receptor-mediated endocytosis

Approximately 2.5×10^5 amebic transformants were incubated in BIS medium containing 2 mg/ml fluorescent fluid-phase marker RITC dextran at 35°C for indicated time points. The cells were collected, washed three times with PBS, and resuspended in 250 µl of lysis buffer (50 mM Tris-HCl, pH 7.5, 150 mM NaCl, and 0.1% Triton-X 100). Fluorescence intensity was measured using a plate reader (SpectraMax Paradigm Multi-Mode, Molecular Devices, California, USA) at an excitation wavelength of 570 nm and an emission wavelength of 610 nm.

Approximately 2×10^4 amebic transformants were incubated in BIS containing 20 µM CellTracker Blue (Thermo Fisher) at 35.5°C for 1 hr. After staining, approximately 10^4 amebic transformants resuspended in 100 µl of BIS medium were transferred to a well on a 96-well glass-bottom plate. After incubation at 35.5°C in an anaerobic chamber for 40 min, 0.5 mg/ml of transferrin conjugate with Alexa Fluor 568 was added to the well and images were acquired by CQ1 and analyzed as above.

Migration (motility) assay

Amoebic trophozoites grown in the logarithmic growth phase were harvested and labelled with 20 μM CellTracker Green for 1 hr at 35.5°C. After washing 3 times with PBS, cells were transferred to a well on a 96-well glass-bottom plate and time lapse images were captured on CQ1. The motility of the cells was measured using CellPathfinder software.

Quantitative real-time (qRT) PCR

The relative levels of mRNA of *EhPTEN1* gene and RNA polymerase II gene, as an internal standard, were measured by qRT-PCR. PCR reaction was prepared using Fast SYBR Master Mix (Applied Biosystems, California, USA) with 100 ng cDNA and a primer set shown in S1 Table. PCR was conducted using the StepOne Plus Real-Time PCR system (Applied Biosystems, California, USA) with the following cycling conditions: an initial step of denaturation at 95°C for 20 sec, followed by 40 cycles of denaturation at 95°C for 3 sec, annealing and extension at 60°C for 30 sec. The mRNA expression level of *EhPTEN1* gene in the transformants was expressed as relative to that in the control transfected with psAP2.

Growth assay of *E. histolytica* trophozoites

Approximately 10^4 trophozoites of *E. histolytica* G3 strain transformed with psAP2-EhPTEN1 and psAP2 (control), grown in the logarithmic phase, were inoculated into 6 ml of fresh BI-S-33 medium containing 10 μg/mL G418, and the parasites were counted every 24 hr on a hemocytometer.

Production of EhPTEN1 recombinant protein

To construct the plasmid for the production of recombinant EhPTEN1 containing a histidine-tag at the amino terminus, the full-length protein coding sequence of *EhPTEN1* gene was amplified by PCR using oligonucleotide primers listed in S2 Table. PCR was performed with PrimeSTAR Max DNA polymerase (Takara Bio Inc, Shiga, Japan) with the following parameters: initial

incubation at 95°C for 1 min; followed by 30 cycles of denaturation at 98°C for 10 sec; annealing at 55°C for 5 sec; and elongation at 72°C for 15 sec; and a final extension at 72°C for 30 sec. The PCR fragment was digested with *Bam*HI and *Sal*I and ligated into *Bam*HI and *Sal*I double digested pCOLD-1 vector (Takara Bio Inc, Shiga, Japan) to produce pCOLD1-EhPTEN1 plasmid. The pCOLD-1-EhPTEN1 was introduced into *E. coli* BL21 (DE3) cells by heat shock at 42°C for 45 sec. *E. coli* BL21 (DE3) strain harboring pCOLD-1-EhPTEN1 was grown at 37°C in 50 ml of LB medium (BD Difco, New Jersey, USA) in the presence of 100 µg/ml ampicillin. The overnight culture was used to inoculate 500 ml of fresh medium, and the culture was further continued at 37°C with shaking at 220 rpm for approximately 2 hr. When A_{600} absorbance reached 0.6, then 1mM of isopropyl β-D-thio galactopyranoside (IPTG) was added, and cultivation was continued for another 24 hr at 15°C. The *E. coli* cells from the induced culture were harvested by centrifugation at 75,000 rpm for 20 min at 4°C. The cell pellet was washed three times with PBS, re-suspended in 30 ml of the lysis buffer (50 mM Tris–HCl, pH 8.0, 300 mM NaCl, and 0.1% Triton X-100) containing 100 µg/ml lysozyme, and 1 mM phenylmethyl sulfonyl fluoride (PMSF), and incubated at room temperature for 30 min. After incubation, the mixture was sonicated on ice and centrifuged at 13,000 rpm for 20 min at 4°C. The supernatant was mixed with 1 ml of 50% Ni^{2+}-NTA His-bind resin (Qiagen, Hilden, Germany), incubated for 1 hr at 4°C with mild rotatory shaking. The resin that recombinant His-EhPTEN1 bound was washed in a disposal column three times with 5 ml of lysis buffer containing 10-30 mM of imidazole. Bound proteins were eluted with 3 ml each of lysis buffer containing 100-300 mM imidazole to obtain recombinant EhPTEN1. The integrity and the purity of the recombinant protein were confirmed with 10% SDS-PAGE analysis, followed by Coomassie Brilliant Blue staining. Then the protein was concentrated, and the buffer was replaced with 50 mM Tris-HCl, 150 mM NaCl, pH 8.0 using Amicon Ultra 50K

centrifugal device (Millipore, Massachusetts, USA). The protein was stored at -30 °C with 50% glycerol in small aliquots until further use.

Lipid phosphatase assay

EhPTEN1 enzymatic activity was determined by the method previously described [83]. Di-C8 phosphatidylinositol phosphate(s) (PIPs) (Echelon Bioscience, Salt Laken City, USA) were dissolved in 100 mM MOPS, pH 6.0, solution, flash frozen in liquid nitrogen, and stored at -20°C between uses. For determination of pH optimum, the following buffers were used, 100 mM acetate buffer (pH 4.0, pH 4.5, pH 5.0, pH 5,5), 100 mM MOPS buffer (pH 6.0, pH 6.5, pH 7.0), and 100 mM Tris-HCl (pH 7.5, pH 8.0, pH 8.5, pH 9.0). For determination of substrate specificity, a reaction mixture was composed of 25 µl of 100 mM MOPS pH 6.0 containing 5 µg of recombinant EhPTEN1 and 100 µM PIPs. The reaction was carried out at 37°C for 40 min and the produced phosphate was measured using Malachite Green Reagent (Cell Signaling technology, Massachusetts, USA). After incubation for 15 min at room temperature, the absorbance was measured at a wavelength of 630 nm. The Lineweaver Burk Plot was used to calculate the kinetic parameters of EhPTEN1.

Lipid membrane overlay assay

Approximately 6×10^6 trophozoites of GFP-EhPTEN1 expressing strain were harvested, washed with PBS, and concentrated by centrifugation. Approximately one hundred µl of lysis buffer (50 mM Tris-HCl, pH 7.5 150 mM NaCl, and 0.1 % Triton X-100, 1× complete mini, and 0.5 mg/ml E64) was added to the cell pellet. The mixture was incubated on ice for 30 min and centrifuged at 13000 rpm for 5 min. The supernatant was collected and used as the total lysate. GFP-EhPTEN1 was immunoprecipitated using GFP-Trap Agarose Kit (ChromoTek, Planegg, Germany) according to the manufacturer's instruction, eluted, and confirmed by immunoblot. Lipid

membranes on which a panel of phospholipids were immobilized (PIP strips: P-6001, Echelon Bioscience, Salt Laken City, USA) were blocked with 1% fat free BSA in PBS-T (PBS containing 0.05% Tween 20) for 1 hr at room temperature. The membranes were then incubated with 2 ml of lipid binding solution (1% fat free BSA in PBS-T, 1x complete mini, 0.05 mg/ml E64, 20 µl of eluted lysate) for 3 hr at 4C. After the membrane were washed twice with PBS-T at 4ºC, they were reacted with anti-GFP at 1:100 dilution with PBS-T containing 1% fat free BSA (PBS-TB) in for 3 hr at 4C. After incubation with the first antibody, the membranes were further reacted with HRP conjugated anti-mouse IgG rabbit antiserum at 1:10,000 dilution with PBS-TB in at 4ºC for 1 hr. The membranes were washed three times with PBS-T at 4ºC and the specific proteins were visualized with a chemiluminescence HRP substrate system (Millipore, Massachusetts, USA) using LAS 4000 (Fujifilm Life Science, Cambridge, USA) according to the manufactures' protocol. Recombinant EhPTEN1 protein was also used except that 1 µg/ml of recombinant protein were incubated on the membrane over night at 4C and anti-His antibody was used as the first antibody with a dilution of 1:1,000.

Acknowledgments

We thank all members of Nozaki lab, particularly Herbert J. Santos, for technical assistance and valuable discussions, and Arif Nurkanto, Emi Mazaki, Kumiko Shibata, Mihoko Imada, and Ratna Wahyuni for all the help and advice.

Figure legends

Fig 1. Structural features and sequence alignments of PTEN in *Entameoba histolytica.* (A) Domain organization of PTEN from human and *E. histolytica.* PDM [PtdIns(4,5)P_2-binding motif],

638 Ptase (Phosphatase tensin-type domain), C2 (C2 tensin-type domain), DUF547 (Domain of
639 unknown function), PDZ-BM (PDZ-binding motif), PEST (proline, glutamine, serine, threonine
640 sequence), red triangle indicates the nuclear localization sequence. **(B)** Relative mRNA expression
641 of PTEN homologs in *E. histolytica* trophozoites HM1: IMSS cl6 and G3 strains. **(C)** Multiple
642 amino acid sequence alignment of human PTEN (P60484), *D. discoideum* PTEN (Q8T9S), and
643 EhPTEN1 (XP_653141.2) was constructed by using clustalw algorithm
644 (http://clustalw.ddbj.nig.ac.jp). PTEN phosphatase domain and C2 domain are shown with blue
645 and yellow backgrounds, respectively. The green rectangle corresponds to the PtdIns(4,5)P_2-
646 binding motif (PDM domain). Amino acid residues implicated for PtdIns(3,4,5)P_3 catalysis are
647 marked with a red rectangle. Cytosolic localization signal and restudies important for TI loop
648 formation are indicated in black and blue lines, respectively. Note that for human PTEN, only the
649 amino terminal part is shown.

650 **Fig 2. Expression and localization of GFP-EhPTEN1 in motile trophozoites. (A)** Immunoblot
651 of GFP-EhPTEN1 and mock control in *E. histolytica* transformants. Approximately 30 μg of total
652 lysates from mock-transfected control (mock) and GFP-EhPTEN1-expressing transformant (GFP-
653 EhPTEN1) were subjected to SDS-PAGE and immunoblot analysis using anti-GFP antibody and
654 anti-CS1 antibody. Arrow indicates GFP-EhPTEN1. **(B)** Live imaging montage showing a time
655 series of motile trophozoites expressing GFP-EhPTEN1. The pseudopodal localization of GFP-
656 EhPTEN1 is indicated by white arrow. The line intensity plot shows GFP-EhPTEN1 intensity in
657 pseudopods vs. cytoplasm with the distance. (Scale bar, 10 μm) **(C)** Relative fluorescence
658 intensities were quantified in the pseudopod regions of GFP-EhPTEN1 and mock control
659 expressing trophozoites then normalized to the fluorescence intensities in the total cells. Data
660 points in the graph show the mean and error bars represent standard deviation for 30 cells.

Statistical significance was examined with t-test (***P<0.001). **(D)** Cell motility of mock and GFP-EhPTEN1 transfected strains. Time-lapse images of the transformant trophozoites were collected every sec for 5 min using CQ1 and 30 cells were selected randomly for analysis by CellPathfinder software. The experiments were performed three times independently. Statistical significance was examined with Dunnet test (**P< 0.05).

Fig 3. Localization of GFP-EhPTEN1 during trogocytosis. (A) Time series montage showing the localization of GFP-EhPTEN1 during trogocytosis of live CHO cells by amoebic trophozoites. The site of trogocytosis is marked with arrow. (Scale bar, 10 µm). **(B)** Analysis of GFP-EhPTEN1 intensity along the line drawn at the initial phase of CHO internalization soon after attachment. **(C)** The plot showing the intensity of GFP-EhPTEN1 along the line drawn reveals its enrichment in the tunnel formed during amoebic trogocytosis. **(D)** The graph shows the intensity of GFP-EhPTEN1 at the late phase of trogocytosis soon after closure of the trogocytic cup **(E)** The graph shows the intensity of GFP-EhPTEN1 after the closure of the trogocytic cup.

Fig 4. Localization of GFP-EhPTEN1 phagocytosis of pre-killed CHO cells. (A) Montage of live trophozoite expressing GFP-EhPTEN1 ingesting pre-killed CHO cells by phagocytosis. (Scale bar, 10 µm). **(B)** Analysis of intensity of GFP-EhPTEN1 across the phagocytic cup along the line drawn. **(C)** The plot showing the intensity of GFP-EhPTEN1 along the line drawn across the newly formed phagosome. **(D)** The graph shows the intensity of GFP-EhPTEN1 after phagosome maturation.

Fig 5. Effect of GFP-EhPTEN1 expression on trogocytosis. (A) Trophozoites of mock transfected and GFP-EhPTEN1 expressing strains were incubated with live CHO cells that have been stained with CellTracker Orange to evaluate trogocytosis. The images were taken on CQ1 as described in the materials and methods and analyzed to calculate the average numbers of CHO

684 cell-containing trogosomes per amoeba. **(B)** The volume of the ingested CHO cells was calculated
685 using three-dimensionally reconstituted data. **(C)** The percentage of amoeba trophozoites that
686 ingested live CHO cells. Experiments were conducted three times independently in triplicates and
687 a representative data set is shown. Statistical significance was examined with t-test (*P<0.05,
688 **P<0.01). Error bars indicating standard deviation.

689 **Fig 6. Effect of GFP-EhPTEN1 expression on phagocytosis. (A)** Trophozoites of mock
690 transfected and GFP-EhPTEN1 expressing strains were incubated with heat killed CHO cells that
691 have been stained with CellTracker Orange to evaluate phagocytosis. The images were taken on
692 CQ1 as described in the materials and methods and analyzed to calculate the average numbers of
693 CHO cell-containing phagosomes per amoeba. **(B)** The volume of the ingested CHO cells was
694 calculated using three-dimensionally reconstituted data. **(C)** The percentage of amoeba
695 trophozoites that ingested pre-killed CHO cells. Experiments were conducted three times
696 independently in triplicates and a representative data set is shown. Statistical significance was
697 examined with t-test (*P< 0.05). Error bars indicating standard deviation.

698 **Fig 7. Establishment and phenotypes of EhPTEN1 gene silenced strain. (A)** Confirmation of
699 gene silencing by RT-PCR analysis of mock transfected and EhPTEN1 gene silenced strain (gs)
700 strain. Transcripts of EhPTEN1 and RNA polymerase II genes were amplified by RT-PCR from
701 cDNA isolated from the transformants and examined by agarose gel electrophoresis. **(B)** Relative
702 levels of EhPTEN1 transcripts by qRT-PCR analysis in EhPTEN1gs and mock strains. The
703 transcript levels were normalized against RNA polymerase II and are shown in percentage relative
704 to the transcript level in mock control strain. Data shown are the means ± standard deviations of
705 two biological replicates. Statistical comparison is made by t-test (**P<0.01). **(C)** Growth kinetics
706 of mock and EhPTEN1gs transformants s during 96 h incubation in BI-S-33 medium. Data shown

are the means ± standard deviations of three biological replicates. Statistical comparison is made by t-test (*P<0.05, **P<0.01, ***P<0.001). **(D)** Cell motility of mock transfected and EhPTEN1 gene silenced strains. The indicated transformant trophozoites were pre-stained with CellTracker green and time-lapse images were collected every sec for 2 min using CQ1 and 30 cells were selected randomly for analysis by CellPathfinder software. The experiments were performed three times independently. Statistical significance was examined with Dunnet test (**P<0.05).

Fig 8. The effect of gene silencing of EhPTEN1 on trogocytosis and phagocytosis. (A, C, and E) Trophozoites of mock and EhPTEN1gs strains were prestained with CellTracker Blue were incubated with live CHO cells that have been stained with CellTracker Orange to evaluate trogocytosis. The images were taken on CQ1 as described in the materials and methods. **(B, D, and F)** Trophozoites of mock and EhPTEN1gs strains were prestained with CellTracker Blue were incubated with heat killed CHO cells that have been stained with CellTracker Orange to evaluate phagocytosis. The images were taken on CQ1 as described in the materials and methods. **(A)** The average numbers of CHO cell-containing trogosomes per amoeba. **(B)** The average numbers of CHO cell-containing phagosomes per amoeba. **(C)** The volume of the trogosomes were calculated using three-dimensionally reconstituted data. **(D)** The volume of the phagosomes were calculated using three-dimensionally reconstituted data. **(E)** The percentage of amoeba trophozoites that ingested live CHO cells. **(F)** The percentage of amoeba trophozoites that ingested pre-killed CHO cells. Experiments were conducted three times independently in triplicates. Statistical significance was examined with t-test (*P<0.05, **P<0.01). Error bars indicating standard deviation.

Fig 9. Effect of EhPTEN1 on pinocytosis. (A) The effect of GFP-EhPTEN1 expression on pinocytosis. Trophozoites of mock transfected and GFP-EhPTEN1 expressing strains were assayed for RITC dextran uptake in a time-dependent manner. **(B)** The effect of pinocytosis upon

730 EhPTEN1 silencing in comparison to mock control. Trophozoites of mock and EhPTEN1gs strains
731 were incubated in BI-S-33 medium containing RITC dextran and assayed for its uptake for
732 indicated time points. Experiments were conducted three times independently and statistical
733 significance was examined with t-test (*P<0.05). Error bars indicating standard errors.

734 **Fig 10. Effect of EhPTEN1 on endocytosis. (A)** The effect of GFP-EhPTEN1 expression on
735 endocytosis. Trophozoites of mock transfected and GFP-EhPTEN1 expressing strains were
736 incubated in BI-S-33 medium containing transferrin and images were taken every 10 min for 1 hr
737 by CQ1 as described in the materials and methods. The volume of endosomes was calculated using
738 three-dimensionally reconstituted data. **(B)** The effect of EhPTEN1 gene silencing on endocytosis.
739 Images of mock and EhPTEN1gs transformant trophozoites that have been co-cultivated with
740 transferrin were taken every 10 min for 1 hr by CQ1 as described in the materials and methods.
741 The volume of endosomes was calculated using three-dimensionally reconstituted data. All
742 experiments were conducted three times independently and statistical significance was examined
743 with t-test (*P<0.05). Error bars indicating standard errors.

744 **Fig 11. Substrate specificity and enzymatic activity of EhPTEN1.** Determination of Eh-PTEN1
745 Specific Activity. The specific activity of bacterial recombinant Eh-PTEN1 fusion protein toward
746 a panel of synthetic di-C8-phosphoinositide substrates was determined using a malachite green-
747 based assay for inorganic phosphate. Reactions were carried out in a volume of 25 µl for 40 min
748 at 37°C, then terminated by the addition of 100 µl of malachite green reagent as described in the
749 materials and methods. The absorbance at 630 nm was measured and phosphate released was
750 quantified by comparison to a standard curve of inorganic phosphate. The means ± standard
751 deviations of three independent experiments performed in duplicates are shown.
752

Legends for Supplementary figures

S1 Fig. Live imaging montage showing localization of GFP-EhPTEN1 in normal motile trophozoites. (A-B) Montage showing a time series of motile trophozoites expressing GFP-EhPTEN1 in left panels. The pseudopodal localization of GFP-EhPTEN1 is indicated by white arrow. The right panels show the fluorescence intensity of GFP-EhPTEN1 across the amoebic trophozoites. (Scale bar, 10 µm).

S2 Fig. Live imaging montage showing localization of GFP mock in normal motile trophozoites. (A-C) Montage showing a time series of motile trophozoites expressing GFP in left panels. The pseudopods in different time frames have been analyzed for GFP intensity along the marked arrow line. The right panels show the fluorescence intensity of GFP across the amoebic trophozoites. (Scale bar, 10 µm).

S3 Fig. Expression and localization of HA-EhPTEN1. (A) Immunoblot analysis of HA-EhPTEN1 in *E. histolytica* transformants. Approximately 30 µg of total lysates from mock-transfected control (mock) and HA-EhPTEN1-expressing transformant (HA-EhPTEN1) were subjected to SDS-PAGE and immunoblot analysis using anti-HA antibody. EhCS1 (Cysteine synthase 1) was detected by anti-CS1 antiserum as a loading control. Arrow indicates HA-EhPTEN1. **(B)** Localization of HA-EhPTEN1 in a quiescent state. Immunofluorescence assay (IFA) micrographs of HA-EhPTEN1 expressing trophozoites stained with anti-HA antibody (green). (Scale bar, 5 µm). **(C)** The line intensity plot shows HA-EhPTEN1 intensity in pseudopods vs. cytoplasm with the distance.

S4 Fig. Localization of GFP mock during phagocytosis. (A) Montage of live trophozoite expressing GFP ingesting pre-killed CHO cells by phagocytosis. (Scale bar, 10 µm). **(B-C)** Analysis of intensity of GFP across the phagocytic cup along the line drawn.

776 **S5 Fig. Evaluation of gene expression by RT-PCR analysis of *EhPTEN1* gene silenced**
777 **transformant.** The steady-state levels of transcripts of *E. histolytica* PTEN isoforms and *EhRNA*
778 *pol II* genes were measured in mock and EhPTEN1gs transformants trophozoites. cDNA from the
779 generated cell lines was subjected to 25 cycles of PCR using specific primers mentioned in S2
780 Table. RNA polymerase II served as a control.
781 **S6 Fig. Expression and purification of EhPTEN1 in *E. coli*. (A)** Expression and purification of
782 recombinant EhPTEN1. Protein samples at each step of purification were subjected to 10% SDS-
783 PAGE and the gel was stained with Coomassie Brilliant Blue. **(B)** Immunoblot analysis of purified
784 recombinant EhPTEN1 using anti-His-tag antibody. The recombinant EhPTEN1 in the supernatant
785 was visualized after longer exposure**. (C)** Optimum pH of EhPTEN1. Enzyme specific activity of
786 recombinant EhPTEN1 was measured at various pHs indicated in the figure. The means ± standard
787 errors of three independent experiments are shown.
788 **S7 Fig. Lipid binding specificity of EhPTEN1.** Lipid binding specificity of EhPTEN1 observed
789 by lipid overlay assay. A panel of PIPs and phospholipid spotted in nitrocellulose membrane was
790 incubated with total lysates from GFP-EhPTEN1 and mock expressing transformants, and
791 recombinant His-EhPTEN1. LPA, lysophosphatidic acid; LPC, lysophosphocholine; PE
792 phosphatidylethanolamine; PC, phosphatidylcholine; S1P, sphingosine-1-phosphate, PA,
793 phosphatidic acid; PS, phosphatidylserine.
794 **S8 Fig. Kinetic analysis of EhPTEN1 phosphatase activity. (A)** Saturation Kinetics for
795 EhPTEN1 against PI(3,4,5)P_3, PI(3,5)P_2, and PI(3,4)P_2. Varying amount of PI(3,4,5)P_3, PI(3,5)P_2,
796 and PI(3,4)P_2 were mixed with EhPTEN1 recombinant protein and phosphate release was
797 measured by a malachite green binding assay as mentioned in the materials and methods. **(B)**
798 Double reciprocal plots of the recombinant EhPTEN1. The enzymatic activities were determined

799 with various concentration of PI(3,4,5)P_3, PI(3,5)P_2, and PI(3,4)P_2. Data are shown in means ±
800 standard deviations of duplicate analysis.
801
802 **S1 Table. Percentage of amino acid identity among *E. histolytica* PTEN isoforms and Human**
803 **PTEN by ClustalW multiple sequence alignment score.**
804 **S2 Table. List of primers used in this study. Restriction site marked by bold letter**.
805
806 **S_1 Movie. Live cell imaging showing localization of GFP-EhPTEN1 in the cytoplasm and**
807 **pseudopod like structures formed by trophozoites.** The trophozoites expressing GFP-EhPTEN1
808 proteins were seeded onto 3.5 cm diameter glass bottom dish and then observed using Carl Zeiss
809 LSM780 confocal microscope. (Scale bar, 10 µm)
810 **S_2 Movie. Live cell imaging showing localization of GFP in motile trophozoites.** The
811 trophozoites expressing GFP mock were seeded onto 3.5 cm diameter glass bottom dish and then
812 observed using Carl Zeiss LSM780 confocal microscope. (Scale bar, 10 µm)
813 **S_3 Movie. Live cell imaging showing localization of GFP-EhPTEN1 during trogocytosis.**
814 The trophozoites expressing GFP-EhPTEN1 proteins were co-cultured with CellTracker Orange
815 stained live CHO cells onto 3.5 cm diameter glass bottom dish and then observed using Carl Zeiss
816 LSM780 confocal microscope. (Scale bar, 10 µm).
817 **S_4 Movie. Live cell imaging showing localization of GFP-EhPTEN1 during phagocytosis.**
818 The trophozoites expressing GFP-EhPTEN-1 proteins were co-cultured with CellTracker Orange
819 stained pre-killed CHO cells onto 3.5 cm diameter glass bottom dish and then observed using Carl
820 Zeiss LSM780 confocal microscope. (Scale bar, 10 µm).

S_5 Movie. Live cell imaging showing localization of GFP during phagocytosis. The trophozoites expressing GFP mock were co-cultured with CellTracker Orange stained pre-killed CHO cells onto 3.5 cm diameter glass bottom dish and then observed using Carl Zeiss LSM780 confocal microscope. (Scale bar, 10 μm).

References

1. Di Paolo G, De Camilli P. Phosphoinositides in cell regulation and membrane dynamics. Nature. 2006;12;443(7112):651-7.
2. Balla T. Phosphoinositides: Tiny lipids with giant impact on cell regulation. Physiol Rev. 2013;93(3):1019–137.
3. Sasaki T, Takasuga S, Sasaki J, Kofuji S, Eguchi S, Yamazaki M, et al. Mammalian phosphoinositide kinases and phosphatases. Prog Lipid Res. 2009;48(6):307–43.
4. Maehama T, Dixon JE. The tumor suppressor, PTEN/MMAC1, dephosphorylates the lipid second messenger, phosphatidylinositol 3,4,5-trisphosphate. J Biol Chem. 1998 May 29;273(22):13375-8.
5. Chalhoub N, Baker SJ. PTEN and the PI3-Kinase Pathway in Cancer. Annu Rev Pathol Mech Dis. 2009 Feb 1;4(1):127–50.
6. Maehama T, Taylor GS, Dixon JE. PTEN and myotubularin: novel phosphoinositide phosphatases. Annu Rev Biochem. 2001;70:247-79.
7. Martin-Belmonte F, Gassama A, Datta A, Yu W, Rescher U, Gerke V, et al. PTEN-Mediated Apical Segregation of Phosphoinositides Controls Epithelial Morphogenesis through Cdc42. Cell. 2007 Jan 26;128(2):383-97.

8. Song MS, Salmena L, Pandolfi PP. The functions and regulation of the PTEN tumour suppressor. Nat Rev Mol Cell Biol. 2012;13(5):283–96.

9. Lee YR, Chen M, Pandolfi PP. The functions and regulation of the PTEN tumour suppressor: new modes and prospects. Nat Rev Mol Cell Biol. 2018;19(9):547–62.

10. Liaw D, Marsh DJ, Li J, Dahia PL, Wang SI, Zheng Z, et al. Germline mutations of the PTEN gene in Cowden disease, an inherited breast and thyroid cancer syndrome. Nat Genet. 1997 May;16(1):64-7.

11. Kim JS, Peng X, De PK, Geahlen RL, Durden DL. PTEN controls immunoreceptor (immunoreceptor tyrosine-based activation motif) signaling and the activation of Rac. Blood. 2002;99(2):694–7.

12. Cao X, Wei G, Fang H, Guo J, Weinstein M, Marsh CB, et al. The Inositol 3-Phosphatase PTEN Negatively Regulates Fcγ Receptor Signaling, but Supports Toll-Like Receptor 4 Signaling in Murine Peritoneal Macrophages. J Immunol. 2004;172(8):4851–7.

13. Ximenez C, Moran P, Rojas L, Valadez A, Gomez A. Reassessment of the epidemiology of amebiasis: state of the art. Infect Genet Evol. 2009; 9:1023–1032.

14. Haque R, Huston CD, Hughes M, Houpt E, Petri WA Jr. Amebiasis. N Engl J Med. 2003 Apr 17;348(16):1565-73. doi: 10.1056/NEJMra022710

15. Stanley SL Jr . Amoebiasis. Lancet. 2003; 361: 1025–1034. doi: 10.1016/S0140-6736(03)12830-9.

16. Ralston KS, Petri WA Jr. Tissue destruction and invasion by *Entamoeba histolytica*. Trends Parasitol. 2011 Jun;27(6):254-63. doi: 10.1016/j.pt.2011.02.006

17. Ralston KS, Solga MD, MacKey-Lawrence NM, Somlata, Bhattacharya A, Petri WA. Trogocytosis by *Entamoeba histolytica* contributes to cell killing and tissue invasion. Nature. 2014;508(7497):526–30.

18. Marie C, Petri WA. Regulation of virulence of *Entamoeba histolytica*. Annu Rev Microbiol. 2014;68:493–520.

19. Nakada-Tsukui K, Nozaki T. Immune response of amebiasis and immune evasion by *Entamoeba histolytica*. Front Immunol. 2016;7(MAY):1–13.

20. Nakada-Tsukui K, Watanabe N, Maehama T, Nozaki T. Phosphatidylinositol Kinases and Phosphatases in *Entamoeba histolytica*. Front Cell Infect Microbiol. 2019;9(JUN):1–36.

21. Somlata, Nakada-Tsukui K, Nozaki T. AGC family kinase 1 participates in trogocytosis but not in phagocytosis in *Entamoeba histolytica*. Nat Commun. 2017;8(1):1–12.

22. Nakada-Tsukui K, Okada H, Mitra BN, Nozaki T. Phosphatidylinositol-phosphates mediate cytoskeletal reorganization during phagocytosis via a unique modular protein consisting of RhoGEF/DH and FYVE domains in the parasitic protozoon *Entamoeba histolytica*. Cell Microbiol. 2009;11(10):1471–91.

23. Watanabe N, Nakada-Tsukui K, Nozaki T. Two isotypes of phosphatidylinositol 3-phosphate-binding sorting nexins play distinct roles in trogocytosis in *Entamoeba histolytica*. Cell Microbiol. 2020;22(3):1–16.

24. Penuliar GM, Nakada-Tsukui K, Nozaki T. Phenotypic and transcriptional profiling in *Entamoeba histolytica* reveal costs to fitness and adaptive responses associated with metronidazole resistance. Front Microbiol. 2015;6(MAY):1–17.

25. Nakada-Tsukui K, Tsuboi K, Furukawa A, Yamada Y, Nozaki T. A novel class of cysteine protease receptors that mediate lysosomal transport. Cell Microbiol. 2012;14:1299–1317.

887 26. Furukawa A, Nakada-Tsukui K, Nozaki T. Novel transmembrane receptor involved in
888 phagosome transport of lysozymes and β-hexosaminidase in the enteric protozoan
889 *Entamoeba histolytica*. PLoS Pathog. 2012;8(2). doi: 10.1371/journal.ppat.1002539
890 27. Lee JO, Yang H, Georgescu MM, Cristofano A Di, Maehama T, Shi Y, et al. Crystal
891 structure of the PTEN tumor suppressor: Implications for its phosphoinositide phosphatase
892 activity and membrane association. Cell. 1999;99(3):323–34.
893 28. Yoshioka D, Fukushima S, Koteishi H, Okuno D, Ide T, Matsuoka S, et al. Single-molecule
894 imaging of PI(4,5)P2 and PTEN in vitro reveals a positive feedback mechanism for PTEN
895 membrane binding. Commun Biol. 2020;3(1):1–14.
896 29. Denning G, Jean-Joseph B, Prince C, Durden DL, Vogt PK. A short N-terminal sequence
897 of PTEN controls cytoplasmic localization and is required for suppression of cell growth.
898 Oncogene. 2007 Jun 7;26(27):3930-40.
899 30. Georgescu MM, Kirsch KH, Kaloudis P, Yang H, Pavletich NP, Hanafusa H. Stabilization
900 and productive positioning roles of the C2 domain of PTEN tumor suppressor. Cancer Res.
901 2000;60(24):7033–8.
902 31. Masson GR, Williams RL. Structural mechanisms of PTEN regulation. Cold Spring Harb
903 Perspect Med. 2020;10(3). doi: 10.1101/cshperspect.a036152
904 32. Mirelman D, Anbar M, Bracha R. Epigenetic transcriptional gene silencing in *Entamoeba*
905 *histolytica*. IUBMB Life. 2008;60(9):598–604.
906 33. Pagliarini DJ, Worby CA, Dixon JE. A PTEN-like phosphatase with a novel substrate
907 specificity. J Biol Chem. 2004;279(37):38590–6.
908 34. Taylor GS, Dixon JE. PTEN and Myotubularins: Families of Phosphoinositide
909 Phosphatases. Methods Enzymol. 2003;366(1997):43–56.

910 35. Naguib A, Bencze G, Cho H, Zheng W, Tocilj A, Elkayam E, et al. PTEN functions by
911 recruitment to cytoplasmic vesicles. Mol Cell. 2015;58(2):255–68.
912 36. Allen L-AH. Phosphoinositide3-kinase regulates actin polymerization during delayed
913 phagocytosis of *Helicobacter pylori*. J Leukoc Biol. 2005;78(1):220–30.
914 37. Kamen LA, Levinsohn J, Swanson JA. Differential association of phosphatidylinositol 3-
915 kinase, SHIP-1, and PTEN with forming phagosomes. Mol Biol Cell. 2007;18(7):2463-72.
916 doi: 10.1091/mbc.e07-01-0061.
917 38. Schabbauer G, Matt U, Günzl P, Warszawska J, Furtner T, Hainzl E, et al. Myeloid PTEN
918 Promotes Inflammation but Impairs Bactericidal Activities during Murine Pneumococcal
919 Pneumonia. J Immunol. 2010;185(1):468–76.
920 39. Mondal S, Ghosh-Roy S, Loison F, Li Y, Jia Y, Harris C, et al. PTEN Negatively Regulates
921 Engulfment of Apoptotic Cells by Modulating Activation of Rac GTPase. J Immunol.
922 2011;187(11):5783–94.
923 40. Li Y, Prasad A, Jia Y, Roy SG, Loison F, Mondal S, et al. Pretreatment with phosphatase
924 and tensin homolog deleted on chromosome 10 (PTEN) inhibitor SF1670 augments the
925 efficacy of granulocyte transfusion in a clinically relevant mouse model. Blood.
926 2011;117(24):6702–13.
927 41. Byekova YA, Powell RR, Welter BH, Temesvari LA. Localization of phosphatidylinositol
928 (3,4,5)-trisphosphate to phagosomes in *Entamoeba histolytica* achieved using glutathione
929 S-transferase- and green fluorescent protein-tagged lipid biosensors. Infect Immun.
930 2010;78(1):125–37.

931 42. Koushik AB, Powell RR, Temesvari LA. Localization of phosphatidylinositol 4,5-
932 bisphosphate to lipid rafts and uroids in the human protozoan parasite *Entamoeba*
933 *histolytica*. Infect Immun. 2013;81(6):2145–55.
934 43. Reyes-López M, Piña-Vázquez C, Serrano-Luna J. Transferrin: Endocytosis and cell
935 signaling in parasitic protozoa. Biomed Res Int. 2015;2015. doi: 10.1155/2015/641392
936 44. Reyes-López M, Bermúdez-Cruz RM, Avila EE, De La Garza M. Acetaldehyde/alcohol
937 dehydrogenase-2 (EhADH2) and clathrin are involved in internalization of human
938 transferrin by *Entamoeba histolytica*. Microbiology. 2011;157(1):209–19.
939 45. Welter BH, Powell RR, Laughlin RC, McGugan GC, Bonner M, King A, et al. *Entamoeba*
940 *histolytica*: Comparison of the role of receptors and filamentous actin among various
941 endocytic processes. Exp Parasitol. 2006;113(2):91–9.
942 46. López-Soto F, León-Sicairos N, Reyes-López M, Serrano-Luna J, Ordaz-Pichardo C, Piña-
943 Vázquez C, et al. Use and endocytosis of iron-containing proteins by *Entamoeba*
944 *histolytica* trophozoites. Infect Genet Evol. 2009;9(6):1038–50.
945 47. Bohdanowicz M, Grinstein S. Role of phospholipids in endocytosis, phagocystosis, and
946 macropinoctosis. Physiol Rev. 2013; 93: 69 106. doi:10.1152/physrev.00002.2012
947 48. Schink KO, Tan KW, Stenmark H. Phosphoinositides in control of membrane
948 dynamics. Annu. Rev. Cell Dev. Biol. 2016; 32:143–71. doi: 10.1146/annurev-cellbio-
949 111315-125349
950 49. Abe N, Inoue T, Galvez T, Klein L, Meyer T. Dissecting the role of PtdIns(4,5)P2 in
951 endocytosis and recycling of the transferrin receptor. J Cell Sci. 2008 May 1;121(Pt
952 9):1488-94. doi: 10.1242/jcs.020792.

953 50. Das K, Watanabe N, Nozaki T. Two StAR-related lipid transfer proteins play specific roles
954 in endocytosis, exocytosis, and motility in the parasitic protist *Entamoeba histolytica*.
955 PLoS Pathog. 2021; 17:1–27.
956 51. Fujii M, Kawai K, Egami Y, Araki N. Dissecting the roles of Rac1 activation and
957 deactivation in macropinocytosis using microscopic photo-manipulation. Sci Rep.
958 2013;3:1–10.
959 52. Swanson JA. Shaping cups into phagosomes and macropinosomes. Nat Rev Mol Cell Biol.
960 2008;9(8):639–49.
961 53. Temesvari L, Zhang L, Fodera B, Janssen KP, Schleicher M, Cardelli JA. Inactivation of
962 lmpA, encoding a LIMPII-related endosomal protein, suppresses the internalization and
963 endosomal trafficking defects in profilin- null mutants. Mol Biol Cell. 2000;11(6):2019–
964 31. doi: 10.1091/mbc.11.6.2019
965 54. Seastone DJ, Lee E, Bush J, Knecht D, Cardelli J. Overexpression of a novel Rho family
966 GTPase, RacC, induces unusual actin-based structures and positively affects phagocytosis
967 in *Dictyostelium discoideum*. Mol Biol Cell. 1998;9(10):2891–904.
968 55. Seastone DJ, Zhang L, Buczynski G, Rebstein P, Weeks G, Spiegelman G, et al. The small
969 M(r) Ras-like GTPase Rap1 and the phospholipase C pathway act to regulate phagocytosis
970 in *Dictyostelium discoideum*. Mol Biol Cell. 1999;10(2):393–406.
971 56. Veltman DM, Williams TD, Bloomfield G, Chen BC, Betzig E, Insall RH, et al. A plasma
972 membrane template for macropinocytic cups. Elife. 2016;5(DECEMBER2016):24. DOI:
973 10.7554/eLife.20085

974 57. Laughlin RC, McGugan GC, Powell RR, Welter BH, Temesvari LA. Involvement of raft-
975 like plasma membrane domains of *Entamoeba histolytica* in pinocytosis and adhesion.
976 Infect Immun. 2004;72(9):5349–57.
977 58. Reyes-López M, Piña-Vázquez C, Pérez-Salazar E, de la Garza M. Endocytosis, signal
978 transduction and proteolytic cleaving of human holotransferrin in *Entamoeba histolytica*.
979 Int J Parasitol. 2020;50(12):959–67.
980 59. Commisso C, Davidson SM, Soydaner-Azeloglu RG, Parker SJ, Kamphorst JJ, Hackett S,
981 et al. Macropinocytosis of protein is an amino acid supply route in Ras-transformed cells.
982 Nature. 2013 May 30;497(7451):633-7. doi: 10.1038/nature12138.
983 60. Hacker U, Albrecht R, Maniak M. Fluid-phase uptake by macropinocytosis in
984 *dictyostelium*. J Cell Sci. 1997;110(2):105–12.
985 61. Muñoz-Muñoz PLA, Mares-Alejandre RE, Meléndez-López SG, Ramos-Ibarra MA.
986 Bioinformatic analysis of two TOR (Target of rapamycin)-like proteins encoded by
987 *Entamoeba histolytica* revealed structural similarities with functional homologs. Genes.
988 2021;12(8). doi: 10.3390/genes12081139
989 62. Janetopoulos C, Borleis J, Vazquez F, Iijima M, Devreotes P. Temporal and spatial
990 regulation of phosphoinositide signaling mediates cytokinesis. Dev Cell. 2005;8(4):467–
991 77.
992 63. Pramanik MK, Iijima M, Iwadate Y, Yumura S. PTEN is a mechanosensing signal
993 transducer for myosin II localization in *Dictyostelium* cells. Genes to Cells.
994 2009;14(7):821–34.

64. Arhets P, Olivo JC, Gounon P, Sansonetti P, Guillén N. Virulence and functions of myosin II are inhibited by overexpression of light meromyosin in *Entamoeba histolytica*. Mol Biol Cell. 1998;9(6):1537–47.

65. Das S, Dixon JE, Cho W. Membrane-binding and activation mechanism of PTEN. Proc Natl Acad Sci U S A. 2003;100(13):7491–6.

66. Vazquez F, Matsuoka S, Sellers WR, Yanagida T, Ueda M, Devreotes PN. Tumor suppressor PTEN acts through dynamic interaction with the plasma membrane. Proc Natl Acad Sci U S A. 2006;103(10):3633–8.

67. Iijima M, Huang YE, Luo HR, Vazquez F, Devreotes PN. Novel mechanism of PTEN regulation by its phosphatidylinositol 4,5-bisphosphate binding motif is critical for chemotaxis. J Biol Chem. 2004;279(16):16606–13.

68. Wessels D, Lusche DF, Kuhl S, Held P, Soll DR. PTEN plays a role in the suppression of lateral pseudopod formation during *Dictyostelium* motility and chemotaxis. J Cell Sci. 2007;120(15):2517–31.

69. Iijima M, Devreotes P. Sensing of chemoattractant gradients. Cell. 2002;109:599–610.

70. Arai Y, Shibata T, Matsuoka S, Sato MJ, Yanagida T, Ueda M. Self-organization of the phosphatidylinositol lipids signaling system for random cell migration. Proc Natl Acad Sci U S A. 2010;107(27):12399–404.

71. Leslie NR, Batty IH, Maccario H, Davidson L, Downes CP. Understanding PTEN regulation: PIP2, polarity and protein stability. Oncogene. 2008;27(41):5464–76.

72. Kölsch V, Charest PG, Firtel RA. The regulation of cell motility and chemotaxis by phospholipid signaling. J Cell Sci. 2008;121(5):551–9.

1017 73. Tsujita K, Itoh T. Phosphoinositides in the regulation of actin cortex and cell migration.
1018 Biochim Biophys Acta - Mol Cell Biol Lipids. 2015;1851(6):824–31.
1019 74. Labruyère E, Guillén N. Host tissue invasion by *Entamoeba histolytica* is powered by
1020 motility and phagocytosis. Arch Med Res. 2006;37(2):252–7.
1021 75. Manich M, Hernandez-Cuevas N, Ospina-Villa JD, Syan S, Marchat LA, Olivo-Marin JC,
1022 et al. Morphodynamics of the actin-rich cytoskeleton in *Entamoeba histolytica*. Front Cell
1023 Infect Microbiol. 2018;8(MAY):1–16.
1024 76. Thompson JD, Higgins DG, Gibson TJ. CLUSTAL W: Improving the sensitivity of
1025 progressive multiple sequence alignment through sequence weighting, position-specific
1026 gap penalties and weight matrix choice. Nucleic Acids Res. 1994;22(22):4673–80.
1027 77. Diamond LS, Mattern CF, Bartgis IL. Viruses of *Entamoeba histolytica*. I. Identification
1028 of transmissible virus-like agents. J Virol. 1972;9(2):326-41.
1029 78. Bracha R, Nuchamowitz Y, Anbar M, Mirelman D. Transcriptional silencing of multiple
1030 genes in trophozoites of *Entamoeba histolytica*. PLoS Pathog. 2006;2(5):431–41
1031 79. Diamond LS, Harlow DR, Cunnick CC. A new medium for the axenic cultivation of
1032 *Entamoeba histolytica* and other entamoeba. Trans R Soc Trop Med Hyg. 1978;72(4):431–
1033 2.
1034 80. Mi-ichi F, Makiuchi T, Furukawa A, Sato D, Nozaki T. Sulfate activation in mitosomes
1035 plays an important role in the proliferation of *Entamoeba histolytica*. PLoS Negl Trop Dis.
1036 2011;5(8):1–7.
1037 81. Nozaki T, Asai T, Sanchez LB, Kobayashi S, Nakazawa M, Takeuchi T. Characterization
1038 of the gene encoding serine acetyltransferase, a regulated enzyme of cysteine biosynthesis
1039 protist parasites *Entamoeba histolytica* and *Entamoeba dispar*. Regulation and possible

function of the cysteine biosynthetic pathway in *Entamoeba*. J Biol Chem. 1999;274(45):32445–52.

82. Nozaki T, Asai T, Kobayashi S, Ikegami F, Noji M, Saito K, et al. Molecular cloning and characterization of the genes encoding two isoforms of cysteine synthase in the enteric protozoan parasite *Entamoeba histolytica*. Mol Biochem Parasitol. 1998;97(1–2):33–44.

83. Mak LH, Woscholski R. Targeting PTEN using small molecule inhibitors. Methods. 2015;77:63–8.

A

Homo sapiens

Entamoeba histolytica

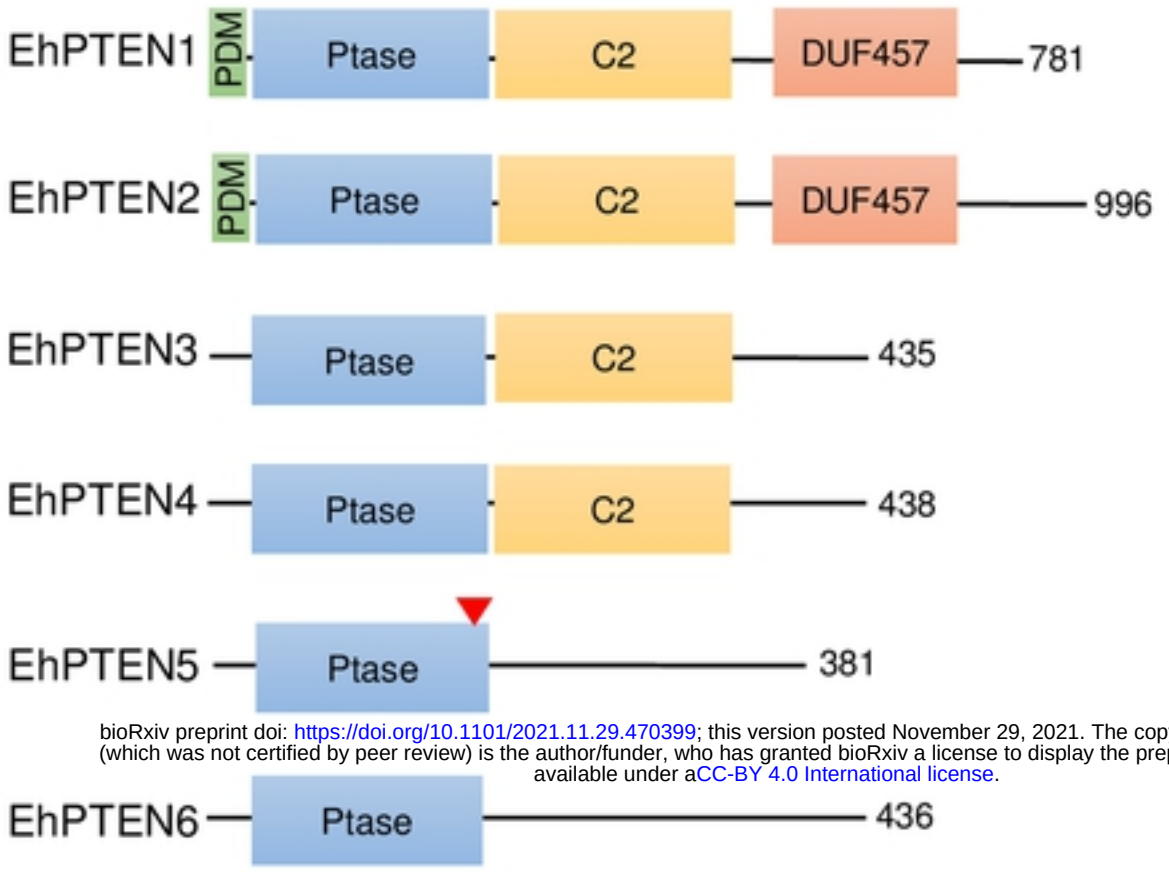

B

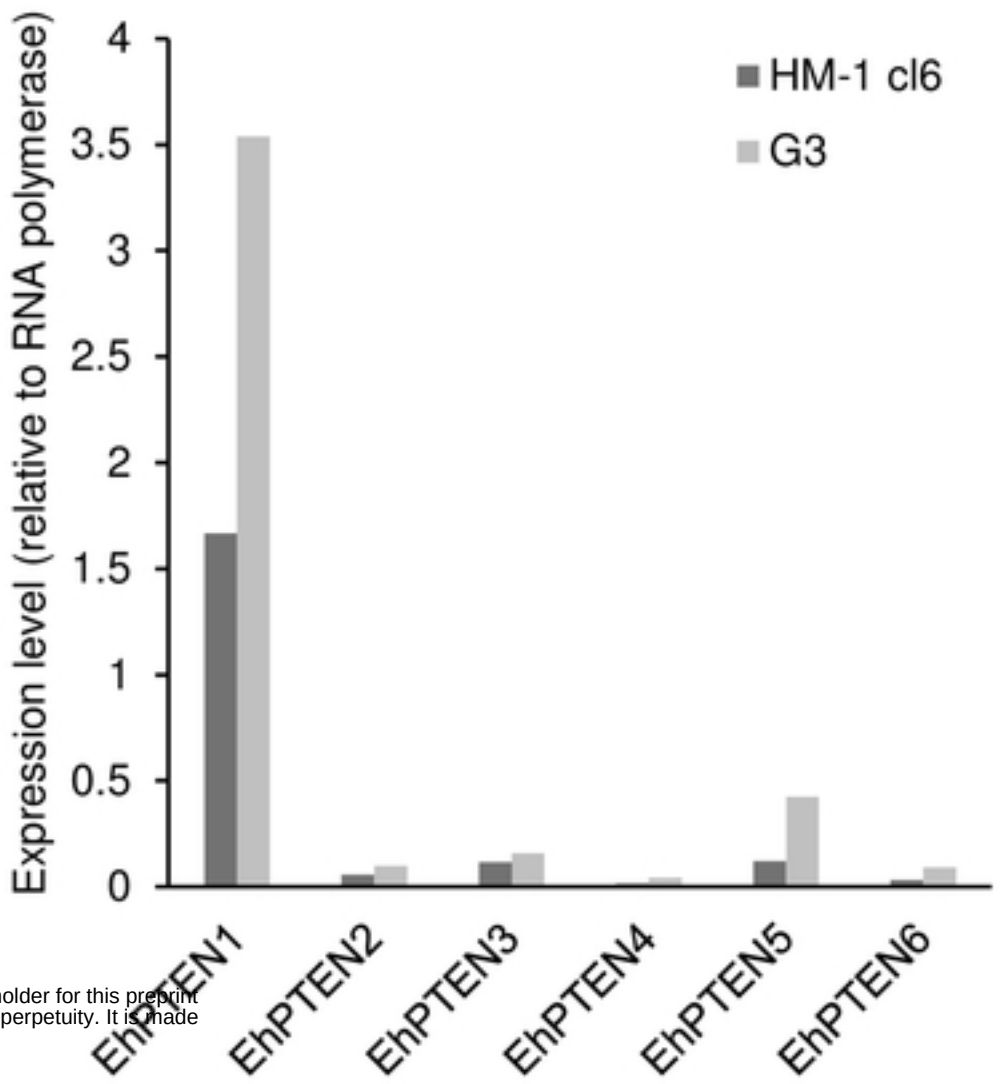

C

```
PTEN_Human                ----------------MTAIIKEIVSRNKRRYQEDGFDLDLTYIYPNIIAMGFPAERLEGVYRNNIDDVVRFLDSKHKNHYKIYNLCAERHYDTA-KFNCRVAQYPFEDHNPPQLELIKPF  104
PTEN_Dictyostelium        ----------------MSNLLRVAVSKQKRRYQKNGYDLDLAYITDNIVAMGFPSEKVEGVFRNPMKDVQRFLDQYHKDHFKVYNLCSERVYDHS-KFYGRVGYYPFDDHNAPQFEMIDAF  104
EhPTEN1                   MKELNNLENLNIHKKMTSVIREAVSKAKRRYQQYGFDLDLSYITPRIIAMGFPSEKFEAAYRNPLVDVLQFFETFHKGHYKVYNFCREKPYDGEHKIKGEYEYFPFDDHNAPEYQIIPQL  120
                                   *: :::  **: *****: *:****:**  .*:*****:*:.*..:** : ** :*::  **.*:*:**:* *: **   *:  .   :**:*** *: ::*  :

PTEN_Human                CEDLDQWLSEDDNHVAAIHCKAGKGRIGVMICAYLLHRGKFLKAQEALDFYGEVRTRDKKGVTIPSQRRYVYYYSYLLKNHLDYRPVALLFHKMMFETIPMFS----------GGTCNP  213
PTEN_Dictyostelium        CRDVDAWMKEDSKNIAVIHCKAGKGRIGLMICCWLMYCGMWKNTEDSLRFYAALRTYNQKGVTIPSQIRYVGYFGRSIRESIKYVPRNVTLKKIVLRPLPKEINLSEVQFNISVGKNCVF  224
EhPTEN1                   CKDVDDYLKADERNVIALHCKAGKGRIGLMSACFLVYMLDSLNAHEAIDFYGTTRTFNKKGVTIPSQLKYINYWSAALKYRFNIGERTVKMVKIEMTPTPRIADEIFVKVST--------  232
                          *.*:* ::. *..:: .:**********:* ..:*::     ::.::: **.  ** ::******** :*: *:.  ::  :.     : : *: :   *

PTEN_Human                -------QFVVCQLKVKI----------------------------------------------------------------------YSSNSGPTRREDKFMYFEFP  244
PTEN_Dictyostelium        NSKEHNMNVVISKKKKTVV----DKNKKDPKKKLTKENSEKNIDSQQQQQSQSSLSQSQQGQSSPNMQSLSASGTISSGSNVGTVNGNTLHQLGGSQFSLSDLADGNTIGNDEYISFEI-  339
EhPTEN1                   ------FNEFVCEKSLTNNRKLTFKPAKDSKNKMKEEDALKLYDEI------------YGELK------EEKGTVSTREAI----------CAWDWKMRCI-EGEDRFGTDGSSFPI-  314
                                 : .:.: . .                                                                                .*     .   * :

PTEN_Human                QPLPVCGDIKVEFFHKQNKMLKKDKMFHFWVNTFFIPGPEETSEKVENGSLCDQEIDSICSIERADNDKEYLVLTLTKNDLDKANKDKANRYFSPNFKVKLYFTKTVEEPSNPEASSSTS  364
PTEN_Dictyostelium        GALSLAGDIRIEFTNKQ-----DDRMFMFWVNTSFVQQLEII----------------------------------PKSGLDKAHKDKNHKAFPEDFHVELTFDQLDQQQSHTTVVASA-  419
EhPTEN1                   DPVTIHGDIKLEFTTSK------GGIFNIWFNTWFIHDNRLEF----------------------------------SKMELDKGF--KDDKQLAPNFKVVLYFEDVTTAPAGEQEMPVCQ  393
                             : : ***::**  .:      . :* :*.** *:   .                                      *  ***.   * .: :  :*:* * * .     :

PTEN_Human                VTP--D--VSDNEPDHYRYSDT--------------TDSDPEN-------------------------------------------------EPFDEDQ----HTQITK------V------  403
PTEN_Dictyostelium        --------EEQTNNQHYPQSSNNVATSSSHHDNITVVASDAPQNNNNNNNNLNSSNSN------NATTT--------TTKNNISL-ASSQSNPVQQESNPSTTTQVSEENSAPKVEAEKIE  516
EhPTEN1                   VGIRTDIPEDVTDPSQVPPMPVSV--------------ACDPNVNAAECLLKETEAVENPKRVKAPTWYPIYHTSLNFKNFERIVSHKIQFPVQREF----------FNINPELDVVK--  487
                                  . .: .:                      *:                                                 *.:.:              :

PTEN_Human                ----------------------------------------------------------------------------------------------------------------  403
PTEN_Dictyostelium        NSNASANDSETSSNSSS------------------------------------------------------------------------------------------------  533
EhPTEN1                   E---TSRDPLEVSRSVLYSIIQLYLRSGFYGRVLDYHIELIMLDNLDGVKLFEQQASELAVINLDNLKTGEHEPFWINVYHIMLLHGLLYWRHRPNIEFKDMLSNFKKFAYKIGGICYTL  604

PTEN_Human                ----------------------------------------------------------------------------------------------------------------  403
PTEN_Dictyostelium        ----------------------------------------------------------------------------------------------------------------  533
EhPTEN1                   HEVLMGCLRQPWPKDSSIDKVVVFDDSNPKSKYAMKEADKSLGCLLSFGTTTSPGIWLYSVEDFAQQKEIAINTYLNRQAAALAAKKEFYLMGNMKMFAKDYGGESNMKRELLARHGVGE  724

PTEN_Human                ----------------------------------------------------------------------------------------------------------------  403
PTEN_Dictyostelium        ----------------------------------------------------------------------------------------------------------------  533
EhPTEN1                   HEIKKWSLKYQPEDRENRIILDHLIAQNIVVTHNPVNFLGQCHLFKYEKPSVKDPKA                                                          781
```

Fig1

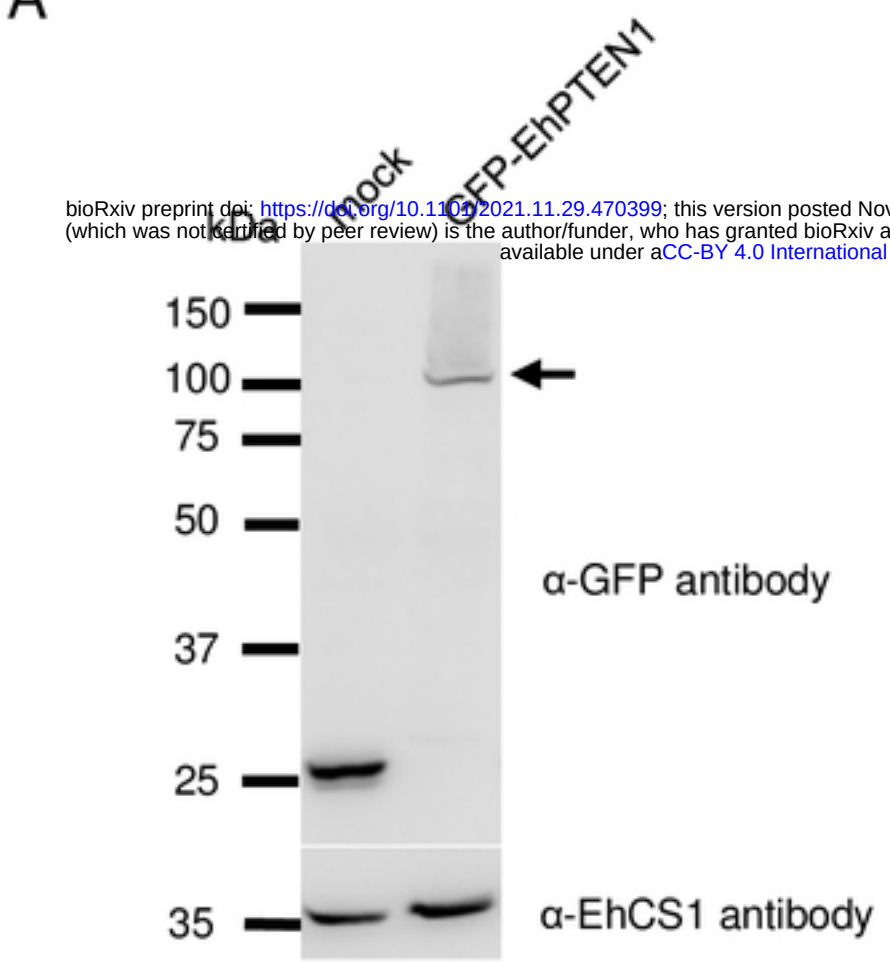

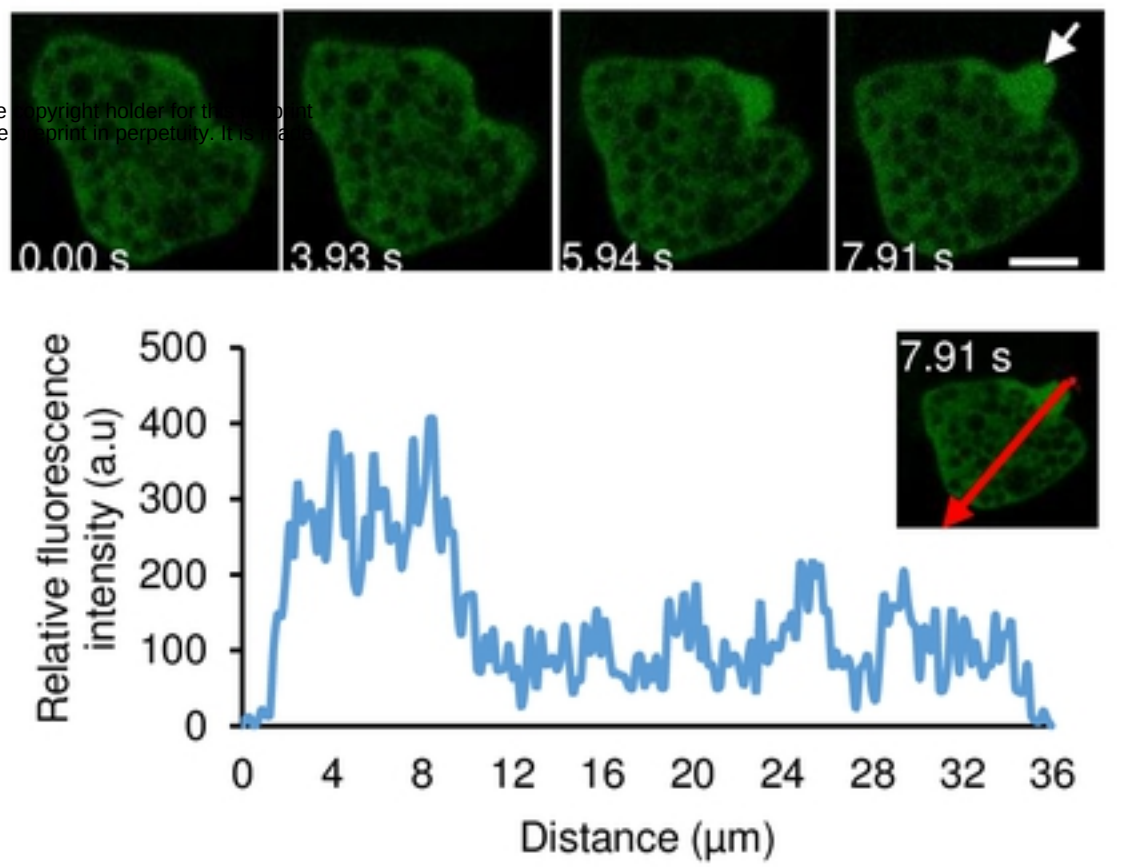

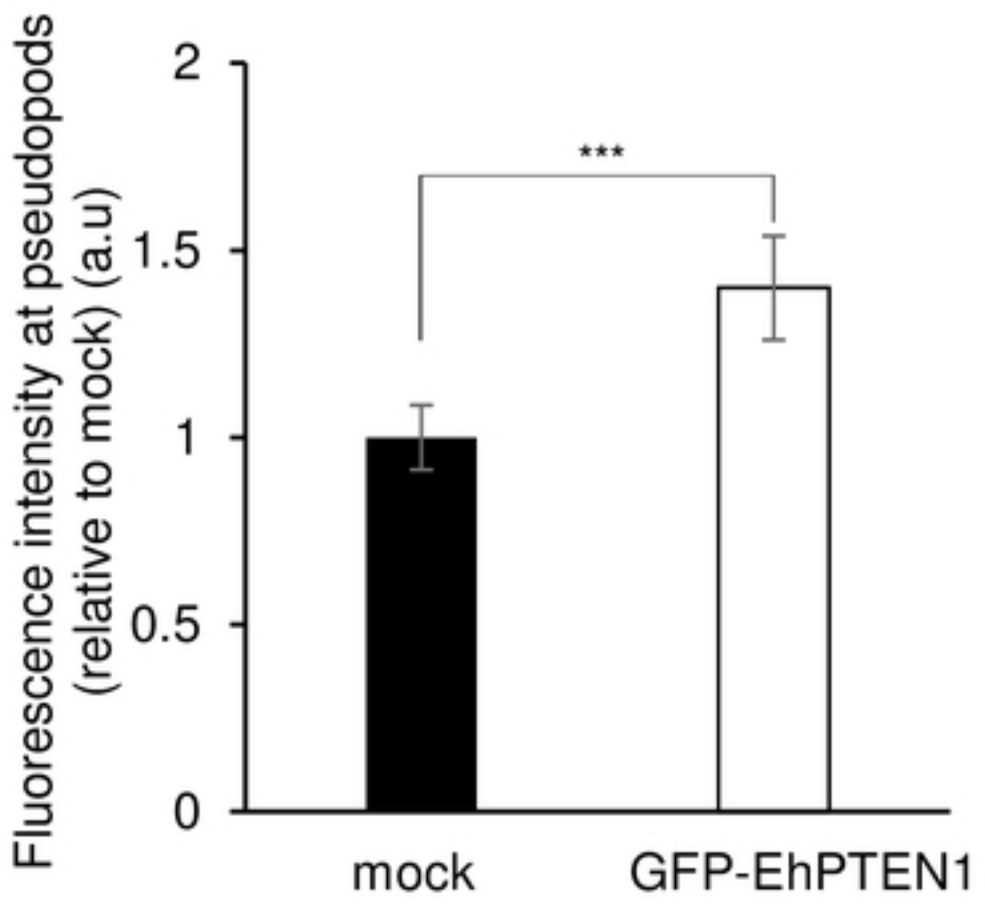

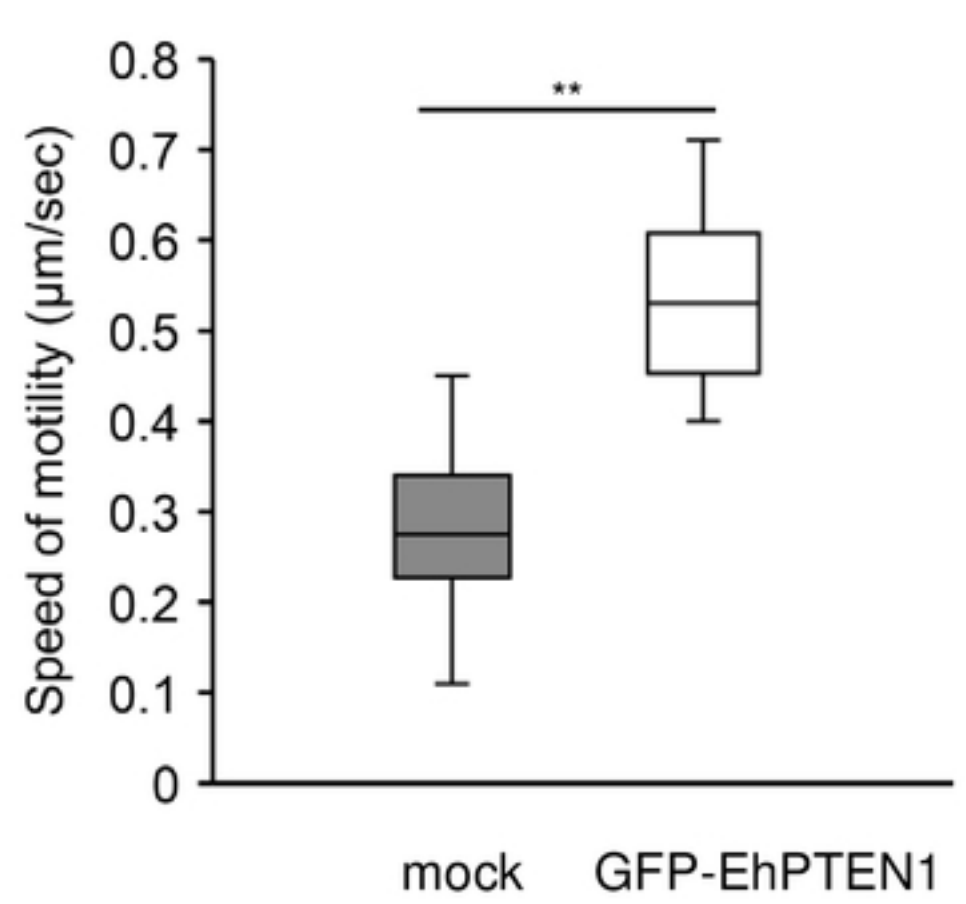

Fig2

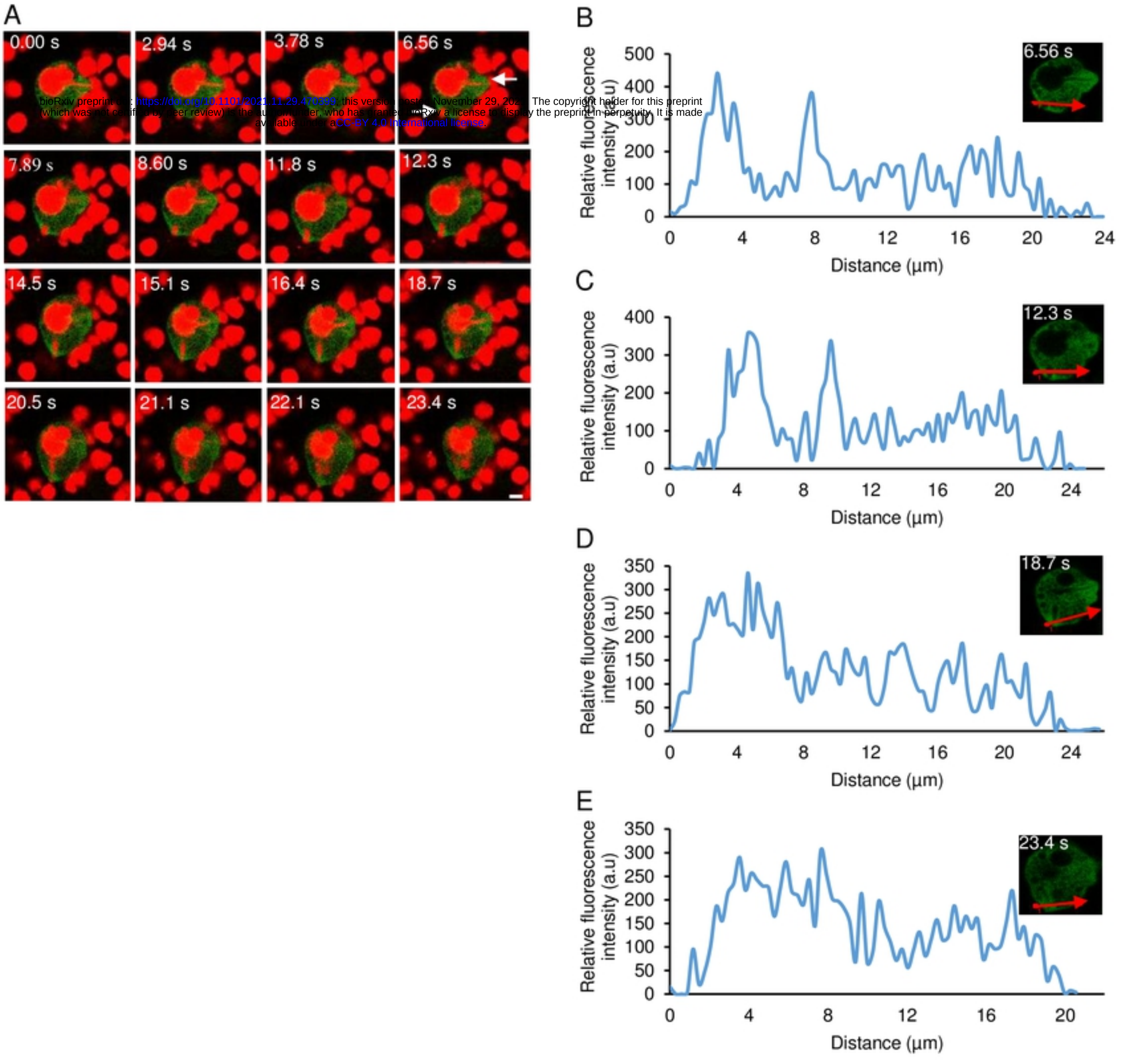

Fig3

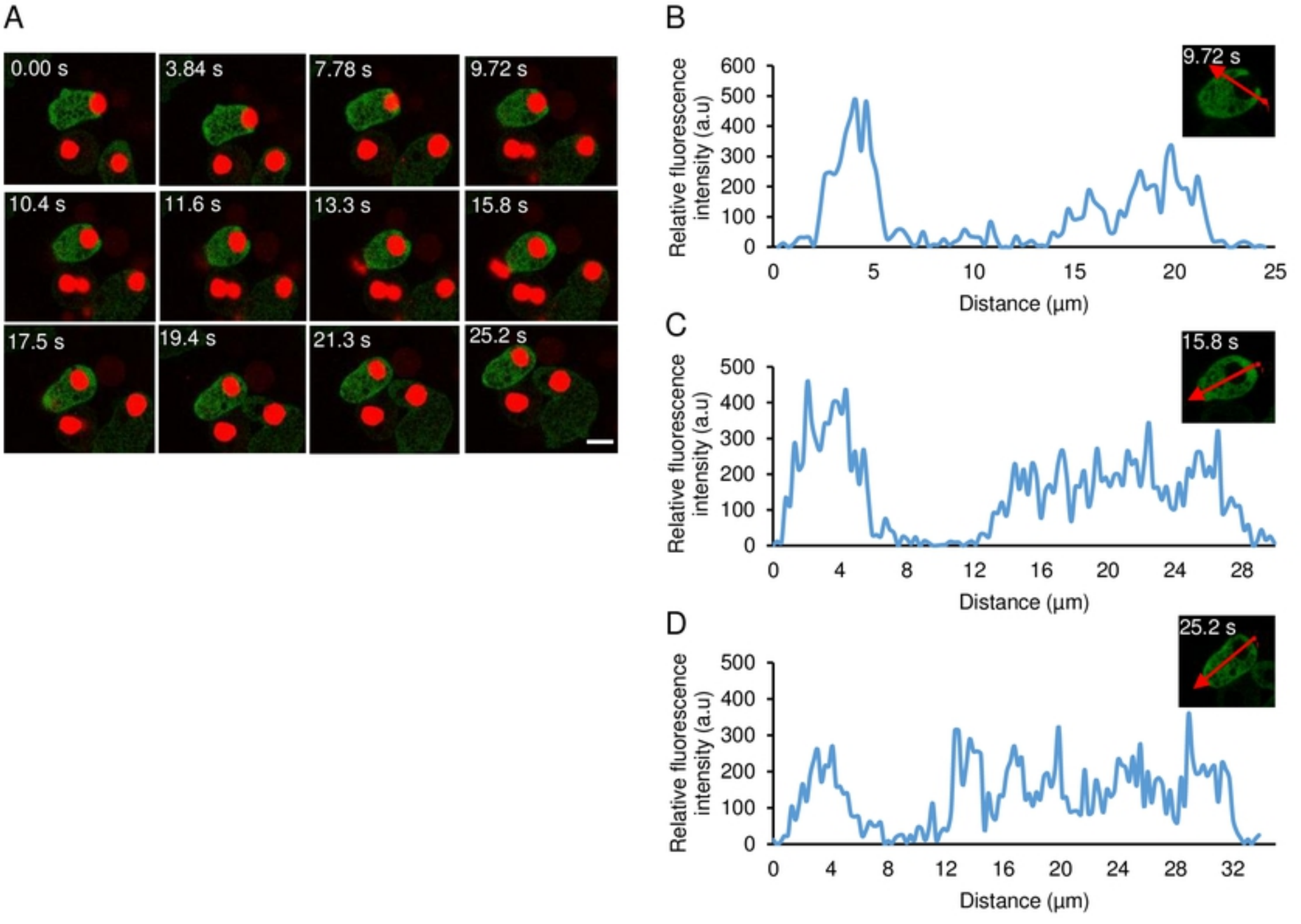
A
0.00 s
3.84 s
7.78 s
9.72 s
10.4 s
11.6 s
13.3 s
15.8 s
17.5 s
19.4 s
21.3 s
25.2 s
B
9.72 s
Relative fluorescence intensity (a.u)
600
500
400
300
200
100
0
0
5
10
15
20
25
Distance (μm)
C
15.8 s
Relative fluorescence intensity (a.u)
500
400
300
200
100
0
0
4
8
12
16
20
24
28
Distance (μm)
D
25.2 s
Relative fluorescence intensity (a.u)
500
400
300
200
100
0
0
4
8
12
16
20
24
28
32
Distance (μm)

Fig4

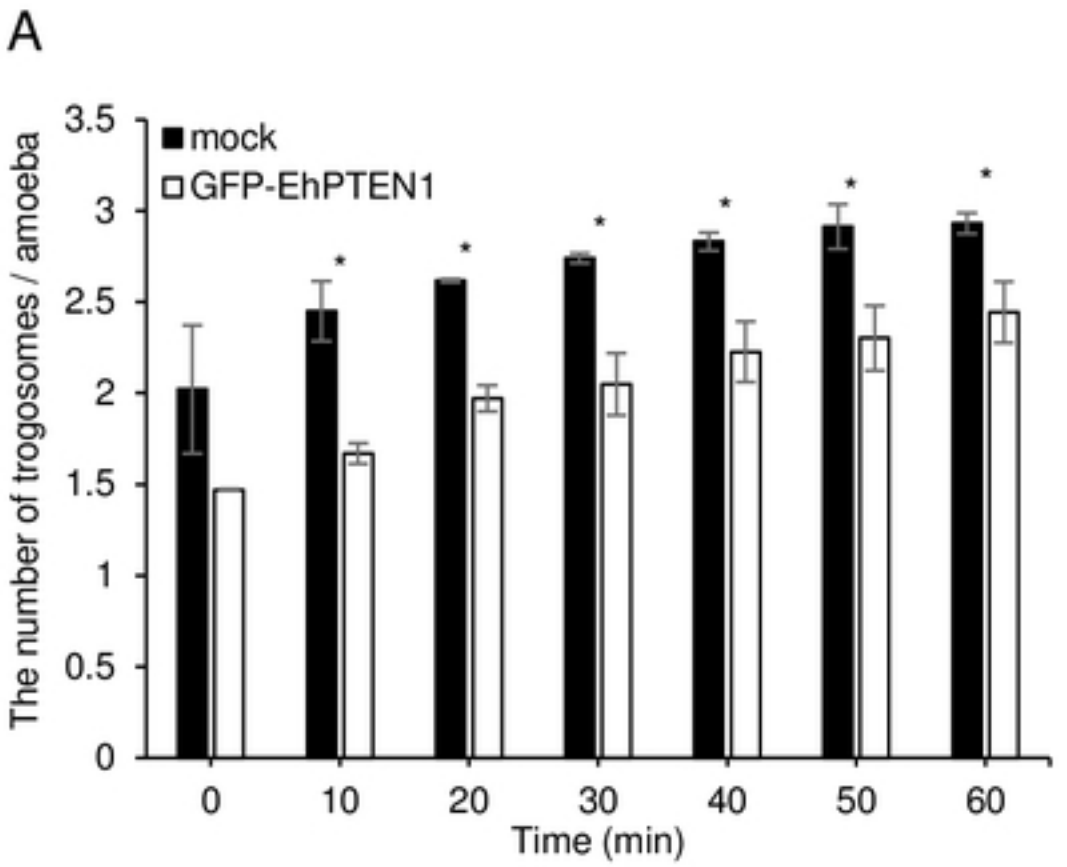

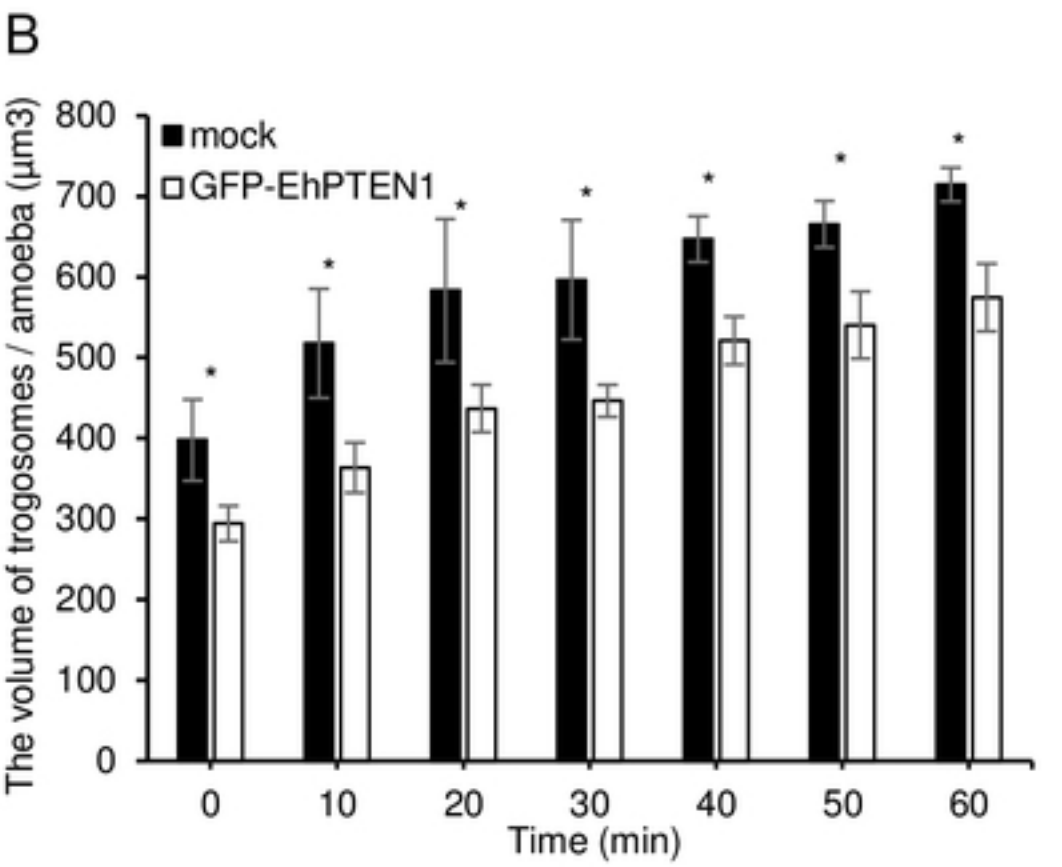

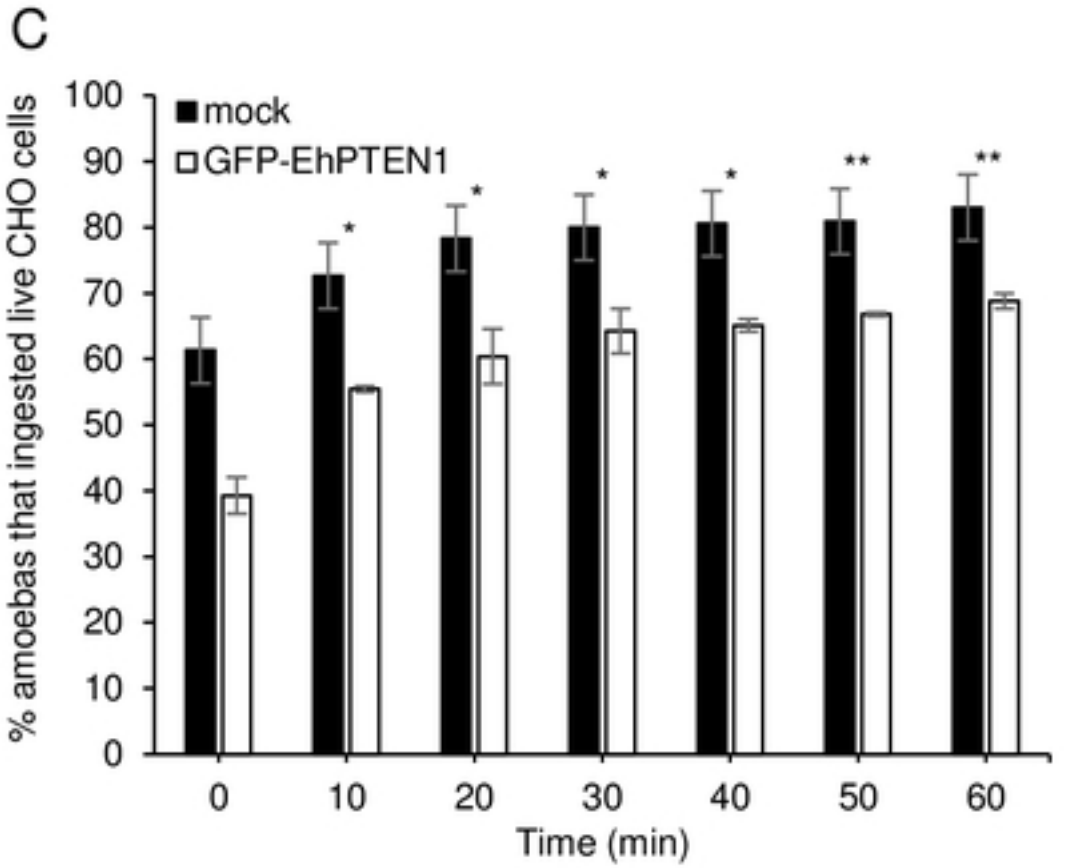

Fig5

A

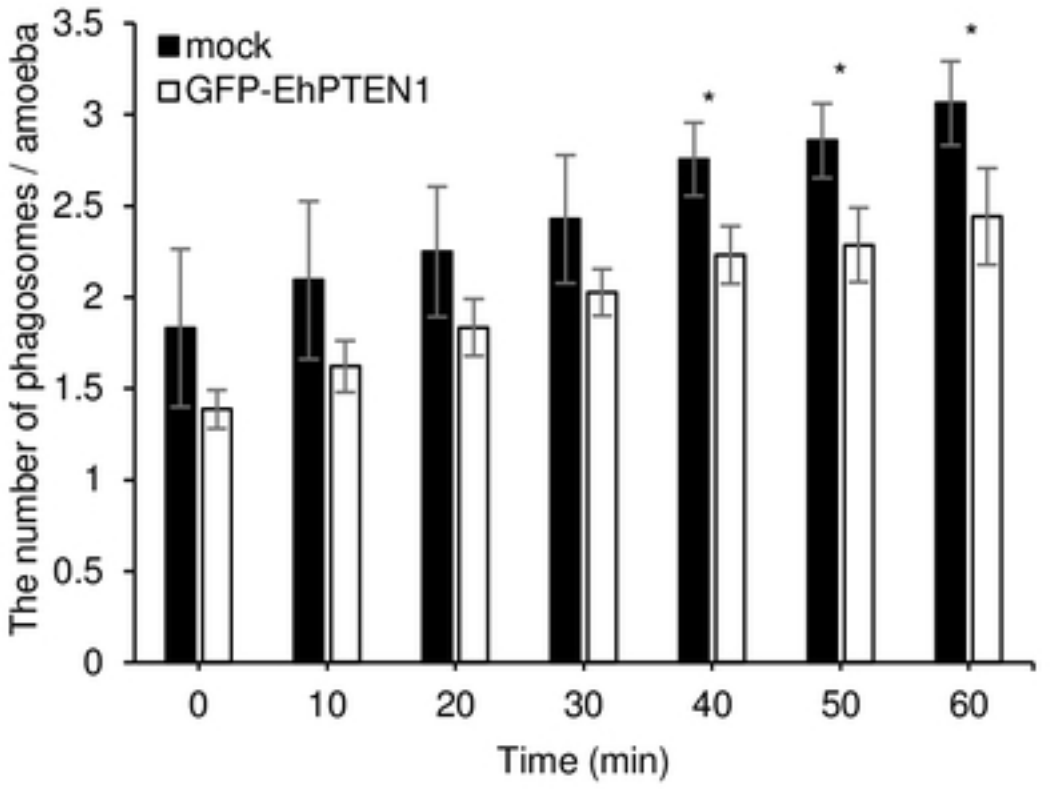
mock
GFP-EhPTEN1
The number of phagosomes / amoeba
3.5
3
2.5
2
1.5
1
0.5
0
0
10
20
30
40
50
60
Time (min)
*
*
*

B

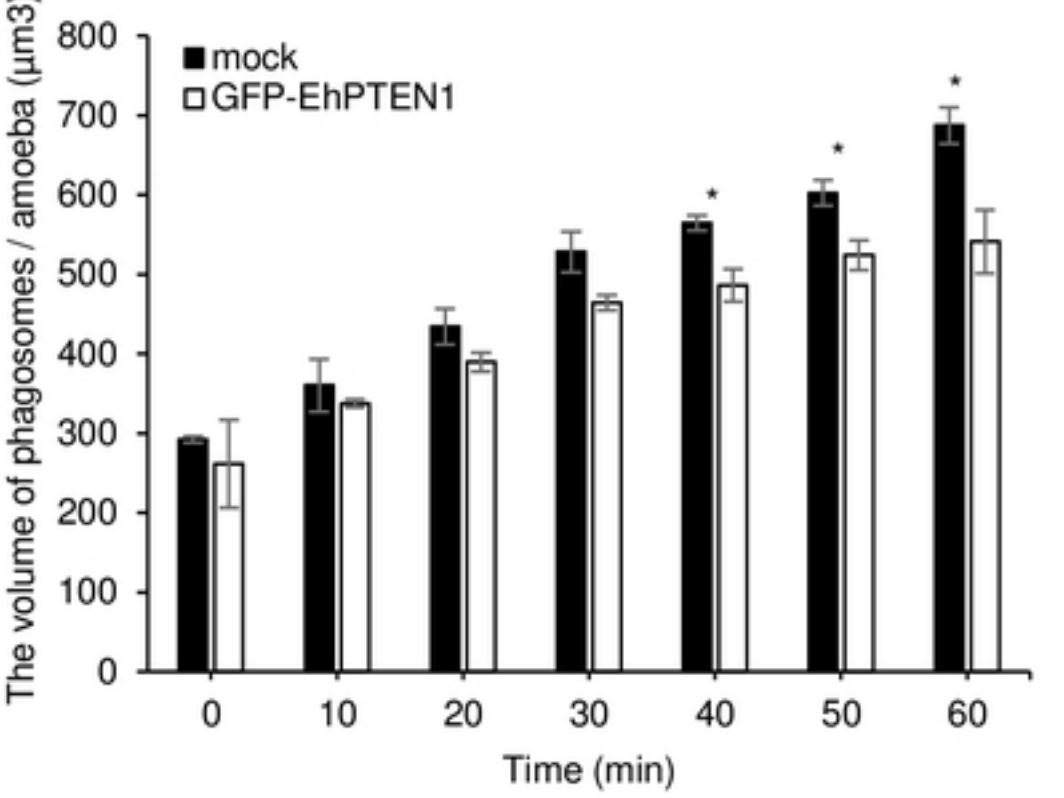
mock
GFP-EhPTEN1
The volume of phagosomes / amoeba (μm3)
800
700
600
500
400
300
200
100
0
0
10
20
30
40
50
60
Time (min)
*
*
*

C

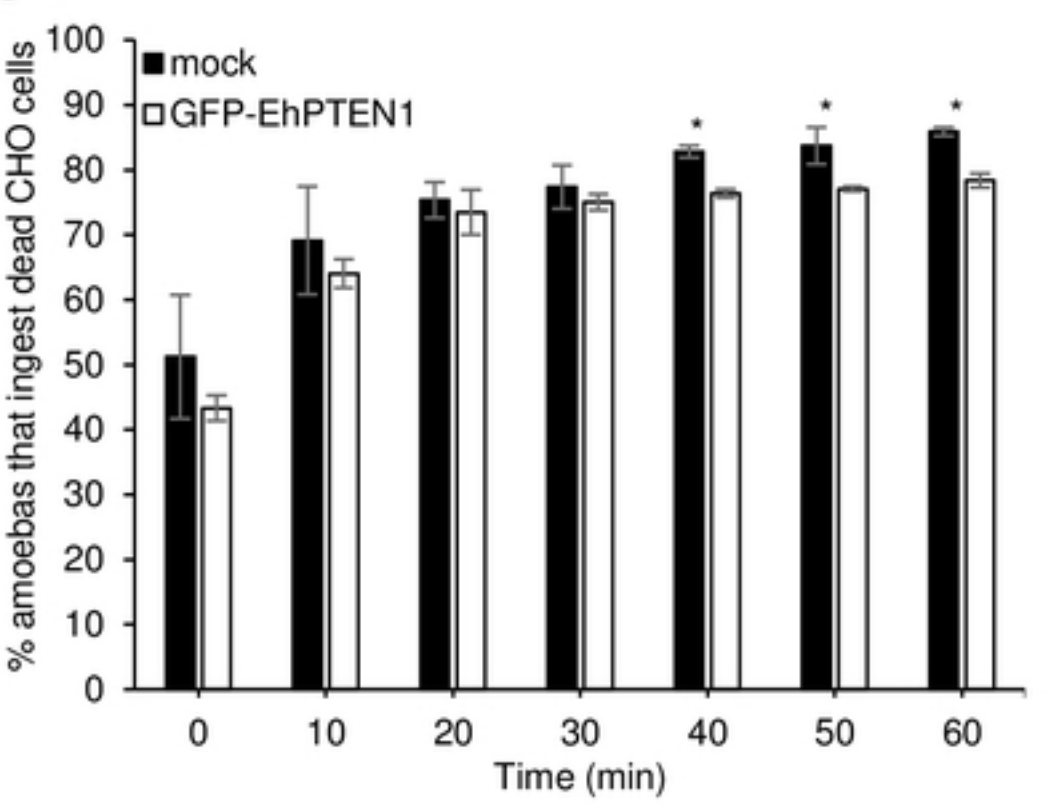
mock
GFP-EhPTEN1
% amoebas that ingest dead CHO cells
100
90
80
70
60
50
40
30
20
10
0
0
10
20
30
40
50
60
Time (min)
*
*
*

Fig6

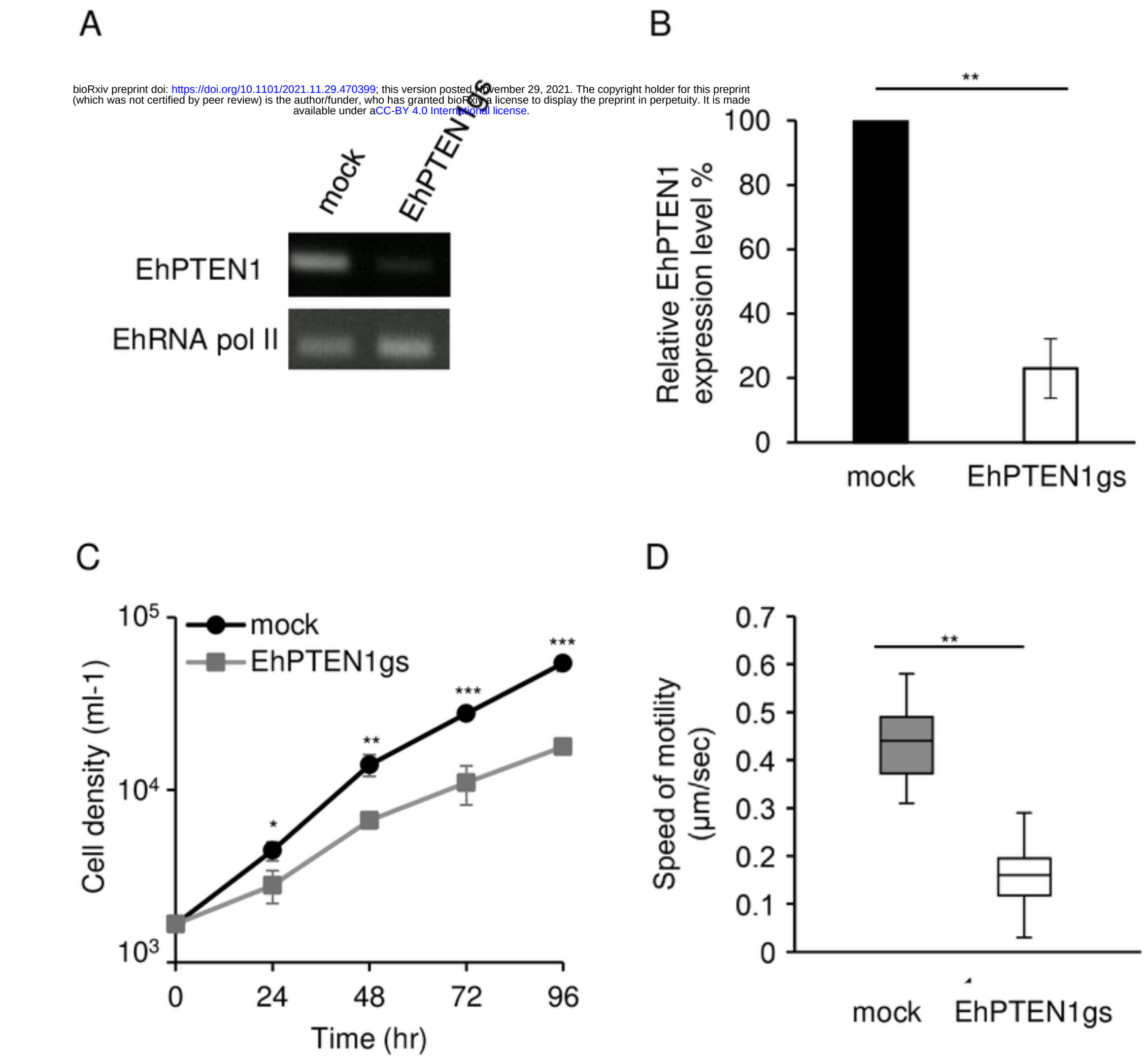

Fig7

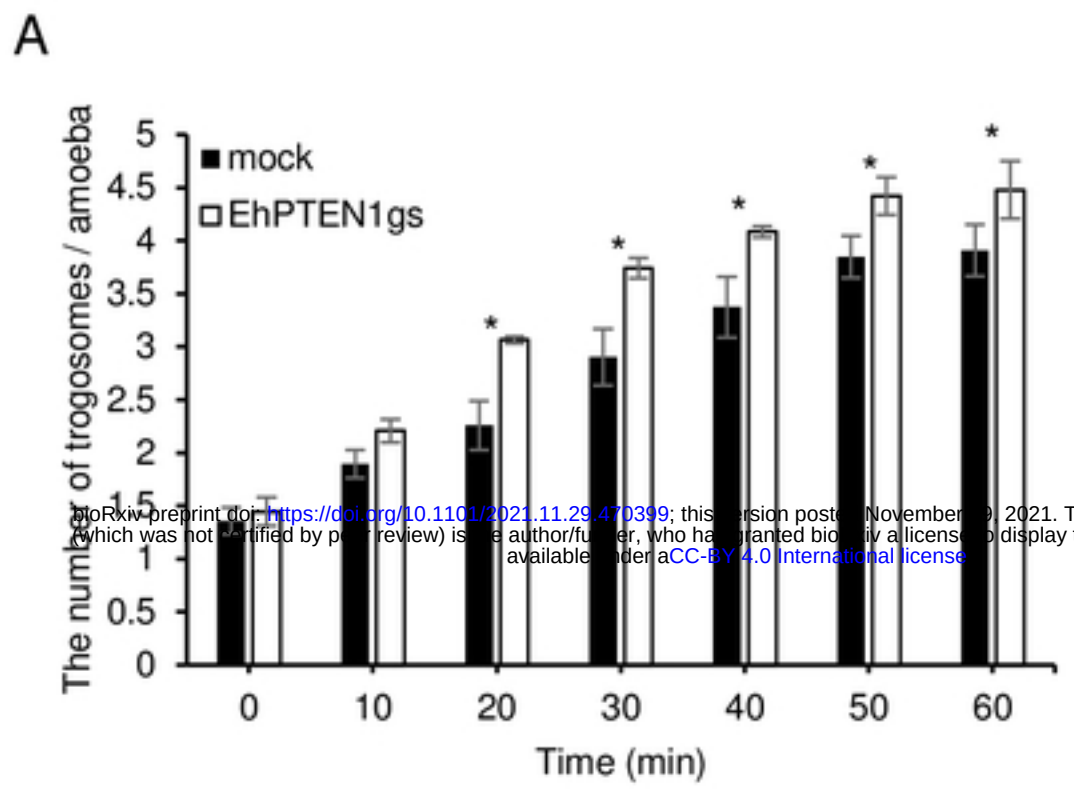

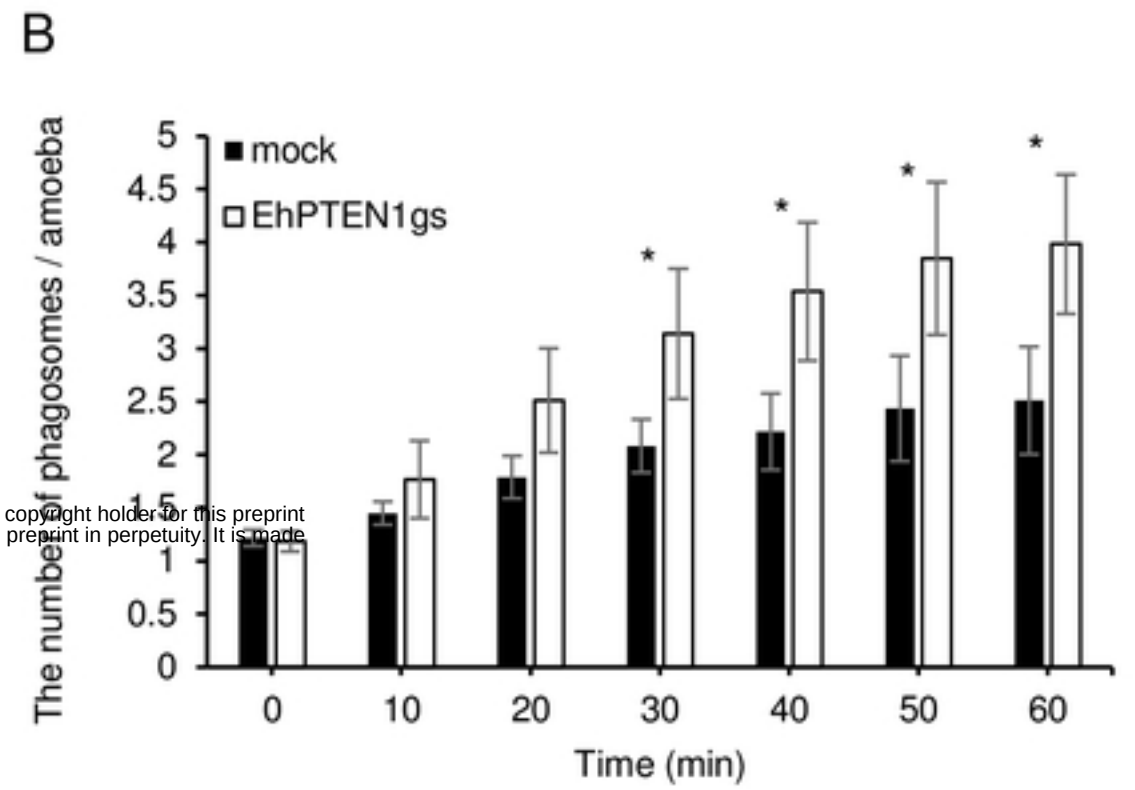

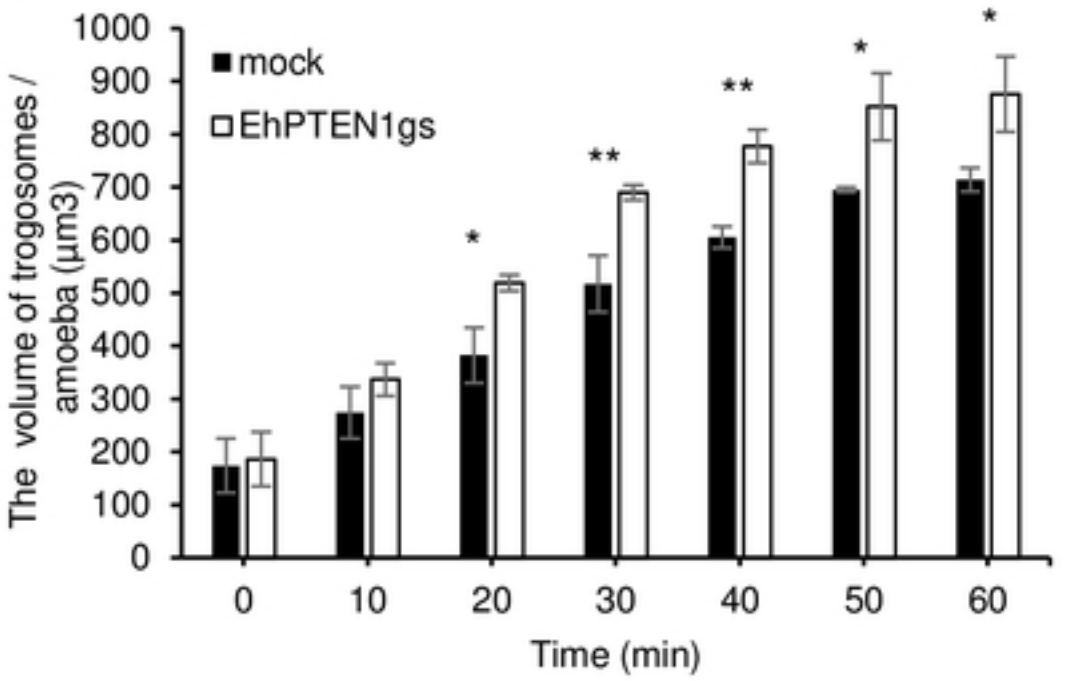

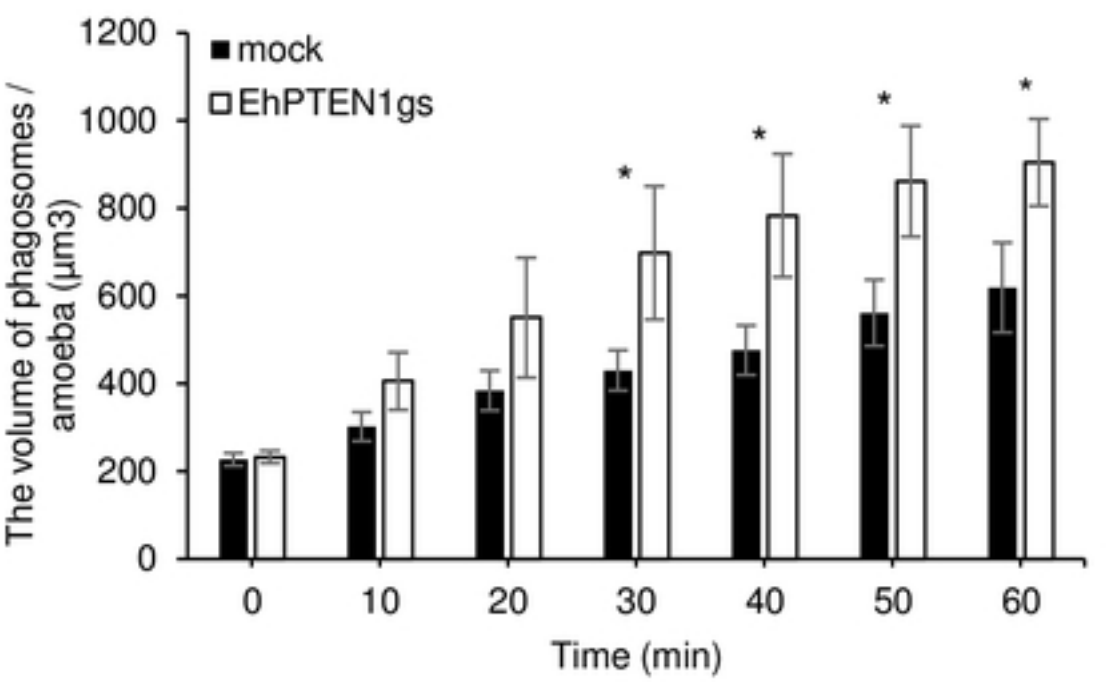

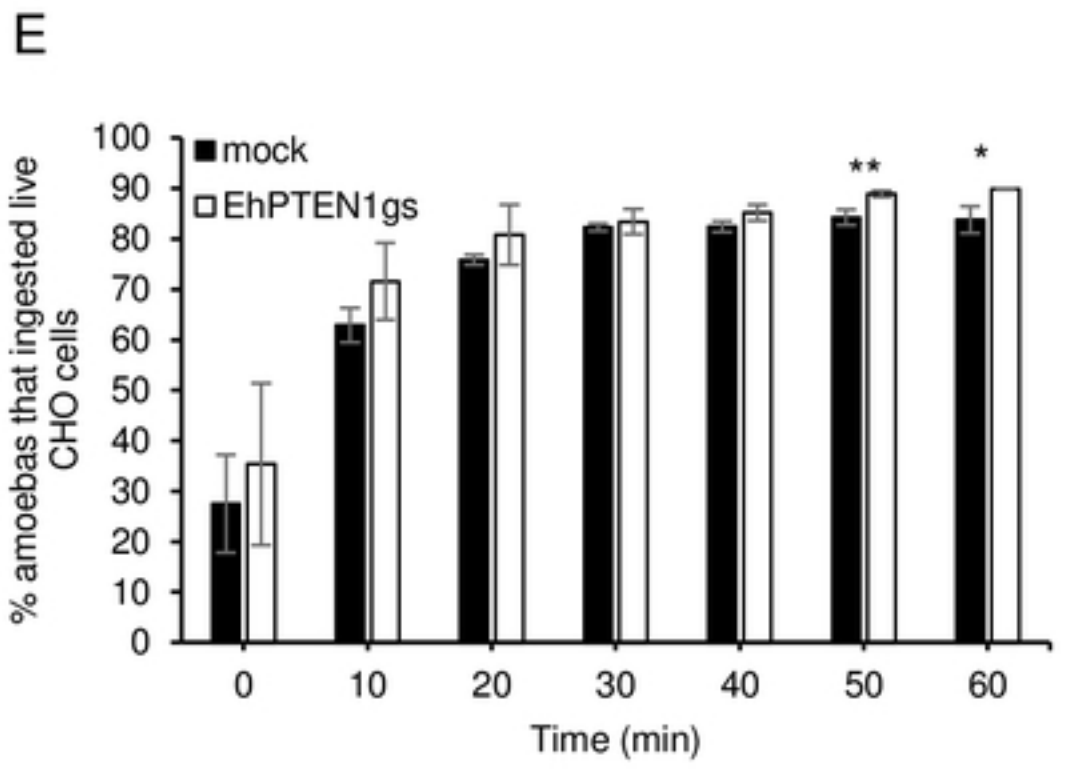

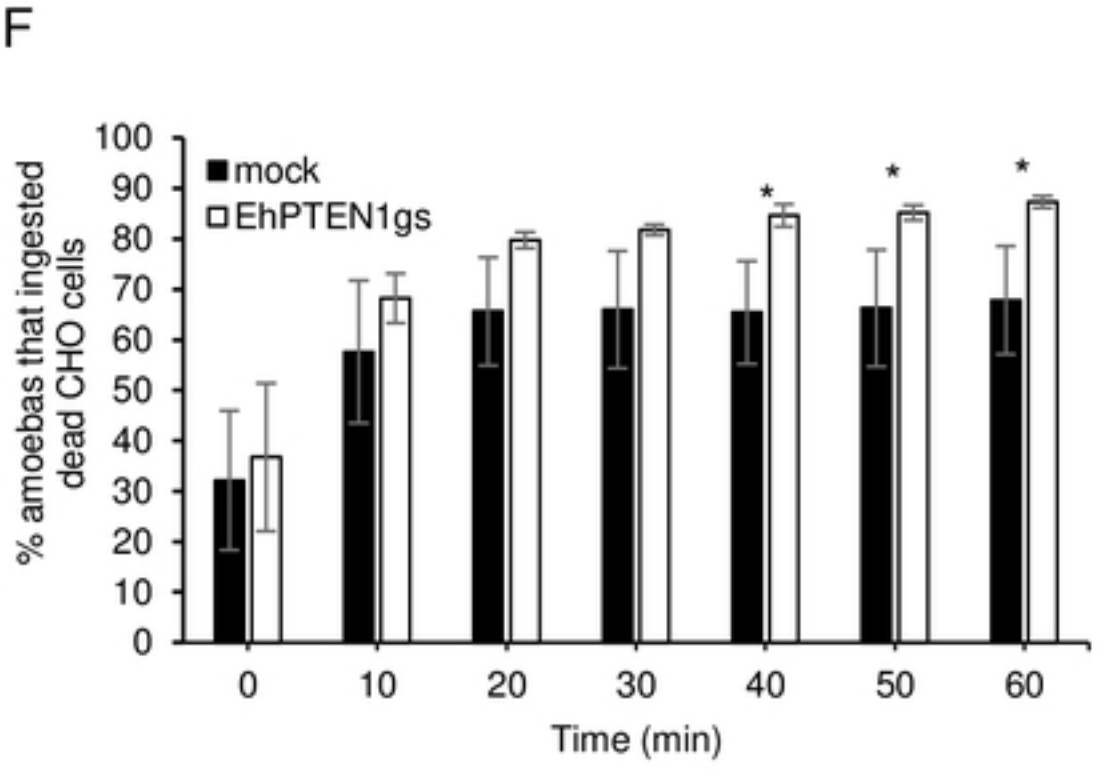

Fig8

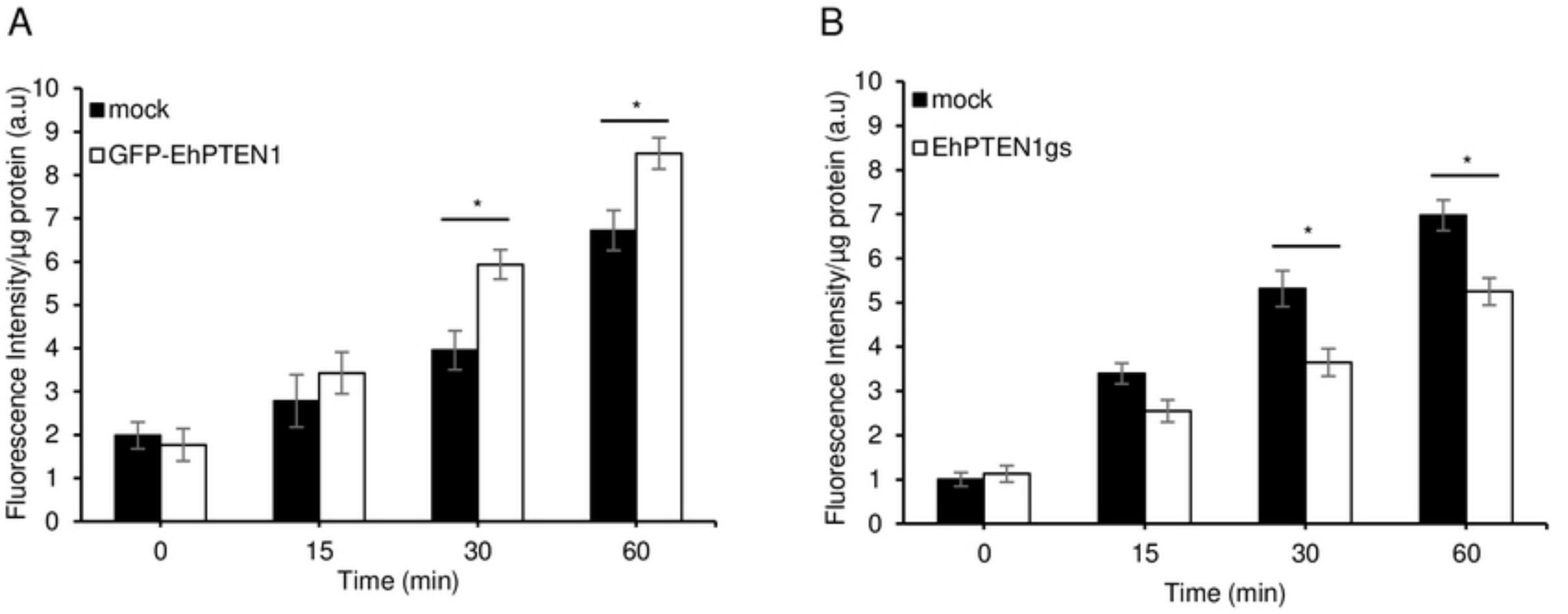
A
mock
GFP-EhPTEN1
Fluorescence Intensity/µg protein (a.u)
Time (min)
0
15
30
60
*
*
B
mock
EhPTEN1gs
Fluorescence Intensity/µg protein (a.u)
Time (min)
0
15
30
60
*
*

Fig9

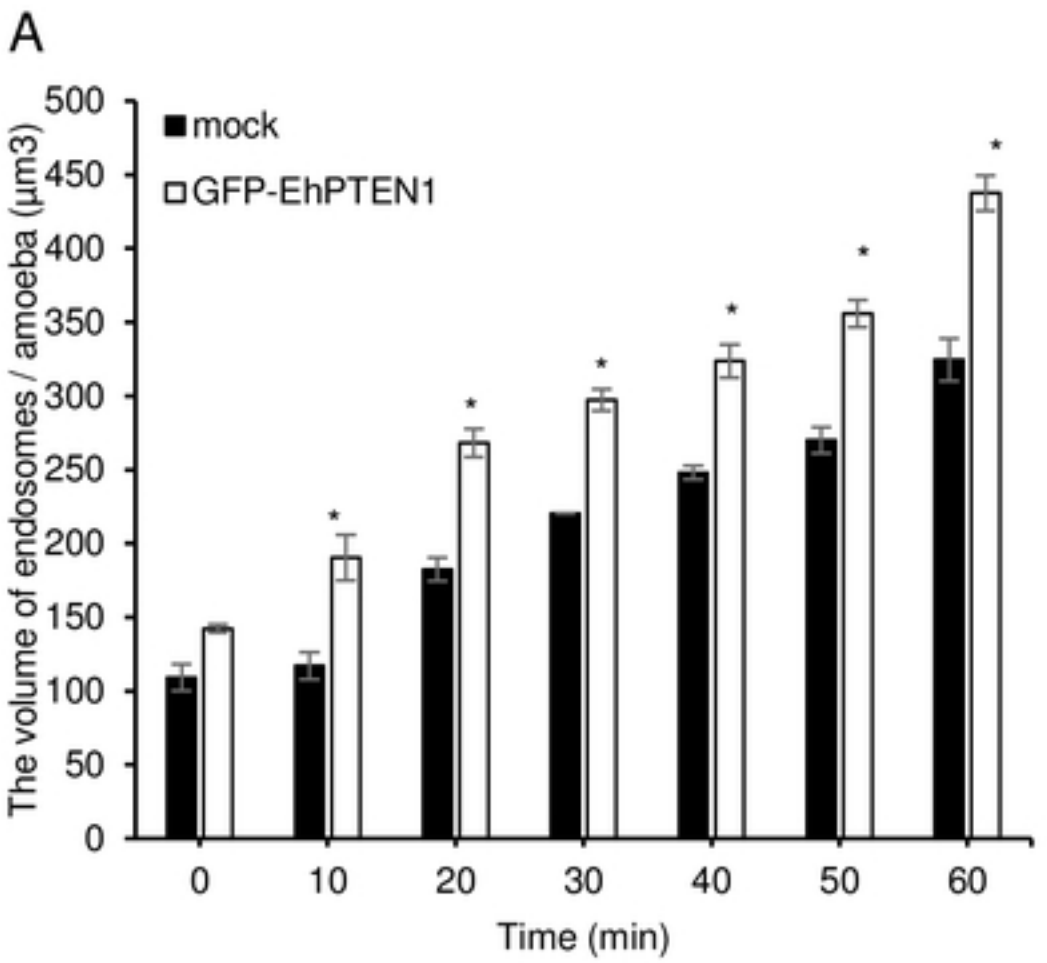
A
mock
GFP-EhPTEN1
The volume of endosomes / amoeba (μm3)
500
450
400
350
300
250
200
150
100
50
0
0
10
20
30
40
50
60
Time (min)
*

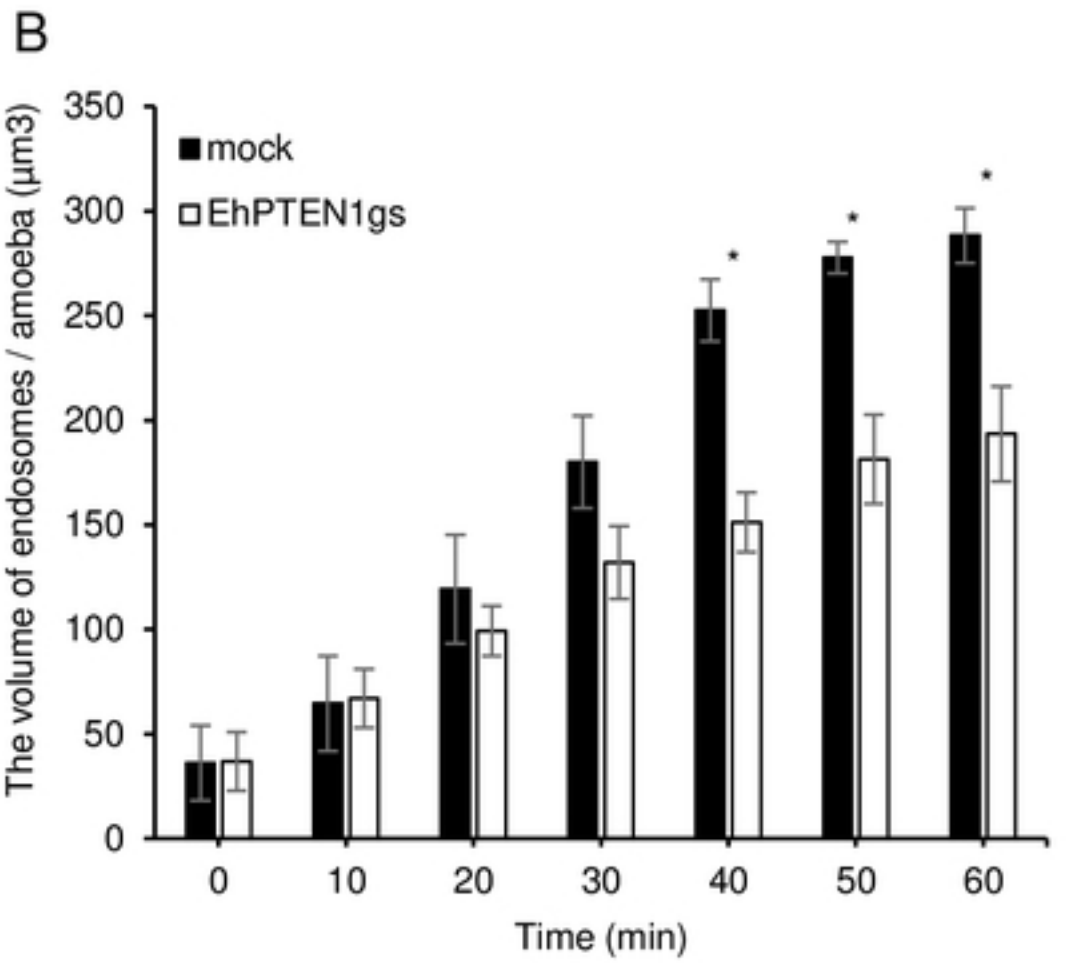
B
mock
EhPTEN1gs
The volume of endosomes / amoeba (μm3)
350
300
250
200
150
100
50
0
0
10
20
30
40
50
60
Time (min)
*

Fig10

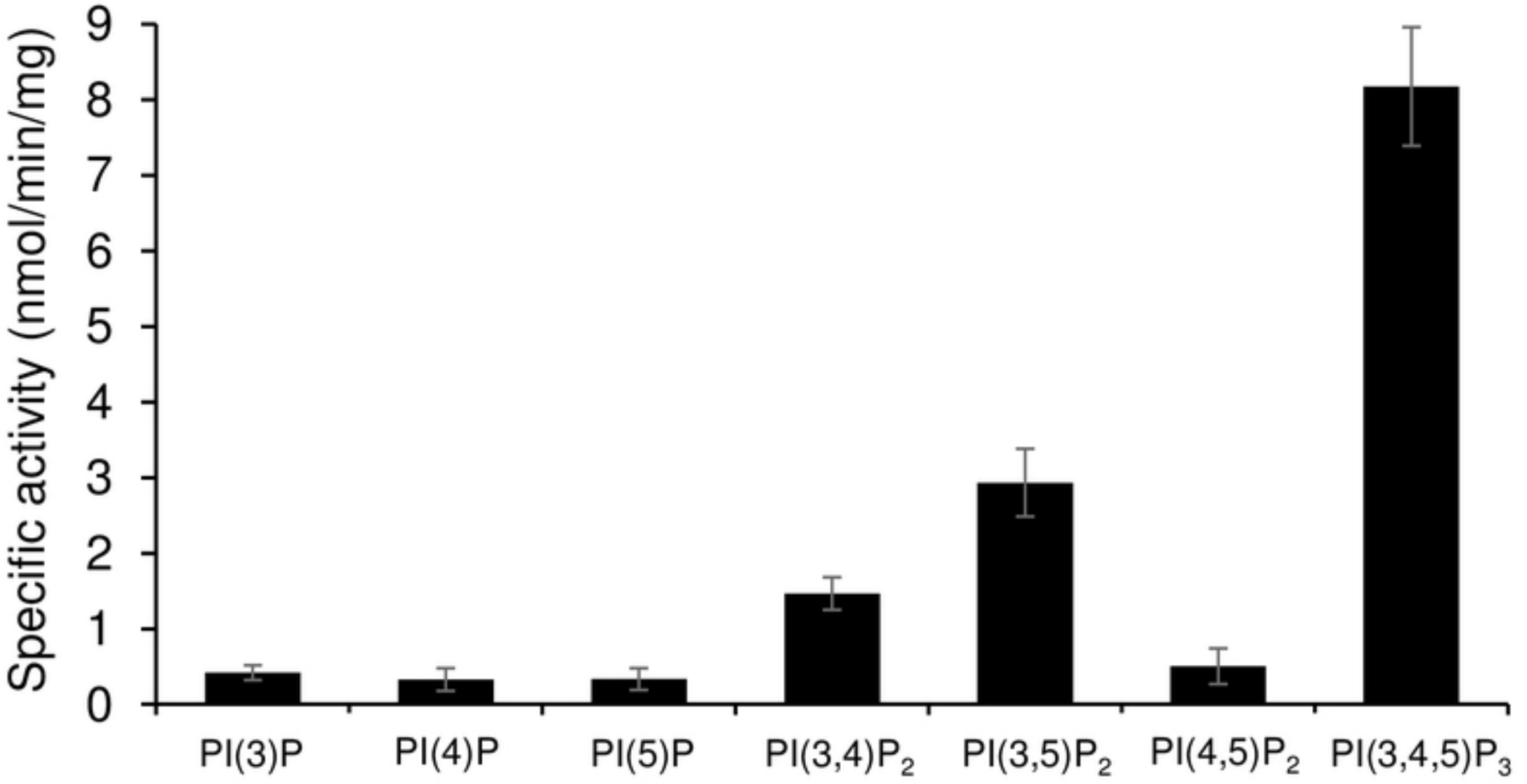
Specific activity (nmol/min/mg)
0
1
2
3
4
5
6
7
8
9
PI(3)P
PI(4)P
PI(5)P
PI(3,4)P2
PI(3,5)P2
PI(4,5)P2
PI(3,4,5)P3

Fig11